DEPARTMENT OF PHYSICS, UNIVERSITY OF JYVÄSKYLÄ
RESEARCH REPORT No. 4/1995

THERMAL DESORPTION MEASUREMENTS OF NOBLE GAS IMPLANTED COPPER

BY
ERKKI KAUTTO

Academic Dissertation
for the Degree of
Doctor of Philosophy

Jyväskylä, Finland
November 1995

URN:ISBN:978-951-39-9826-4
ISBN 978-951-39-9826-4 (PDF)
ISSN 0075-465X

Jyväskylän yliopisto, 2023

ISBN 951-34-0626-1
ISSN 0075-465X

DEPARTMENT OF PHYSICS, UNIVERSITY OF JYVÄSKYLÄ
RESEARCH REPORT No. 4/1995

THERMAL DESORPTION MEASUREMENTS OF NOBLE GAS IMPLANTED COPPER

BY
ERKKI KAUTTO

Academic Dissertation
for the Degree of
Doctor of Philosophy

To be presented, by permission of the
Faculty of Mathematics and Natural Sciences
of the University of Jyväskylä,
for public examination in Auditorium S-212 of the
University of Jyväskylä on November 10, 1995,
at 12 o'clock noon

Jyväskylä, Finland
November 1995

Preface

To my supervisors, Prof. Matti Manninen and Dr. Hannu Rajainmäki I would like to express my gratitude. I also want to thank Dr. Olli-Pekka Kähkönen and Mr. Juha Kuhalainen for a fruitful collaboration during these years. The support and interest obtained from the condensed matter group as a whole is acknowledged.

Most of the work described in this thesis was carried out in the Accelerator Laboratory, University of Jyväskylä. I am indebted to the technical staff of the laboratory for their patient help during the first years of this project. Especially I want to thank Mr. Teuvo Poikolainen and Prof. Kalevi Valli for constructive discussions in the field of vacuum technology.

Finally, I want to thank the Department of Physics for its remarkable investment in the new facility used in this work. The research assistantship granted by the University of Jyväskylä as well as the financial support from the Academy of Finland are greatly acknowledged.

Jyväskylä, November 1995

Erkki Kautto

Abstract

Thermal desorption measurements applied to copper are described. The role of the first-order rate equation and diffusive release are discussed. A critical review of the analysing methods based on first-order kinetics is presented. The facility used for the measurements is described in detail. The experimental results concentrate on the behaviour of noble gas implants in monocrystalline copper. In the case of helium, each peak observed in thermal desorption spectra can be associated with microscopic processes. The dissociation energy of helium in a monovacancy was found to be 2.0 $\pm$ 0.1 eV. The behaviour of argon and neon in copper turned out to be more complicated, and only tentative interpretations can be given. When low-energy helium implants were attempted to use for probing vacancies in copper, no clear evidence of helium-filled monovacancies was found. Therefore the interstitial mechanism was assumed to play a dominating role in the recovery of irradiation damages in copper.

Table of contents

Introduction

During the last three decades much theoretical and experimental work has been devoted to studying the behaviour of noble gases in metals [**1-5**]. The studies were motivated mainly by two different reasons. Firstly, there has been a lot of interest in solving the well-known instability problems caused by noble gases in ion pumps [**6**]. Secondly, the behaviour of helium has to be fully understood in materials that might be used in fusion technology. So far most of the investigations have been concentrated on refractory metals such as tungsten [**3,4,7**] and molybdenum [**8**], i.e. materials with a high strength and a good tolerance against high temperatures.

The unique behaviour of noble gas implants in solids as such has turned out to be worth studying, since such experiments give information about many different interactions in metals. These experiments consist of ion implantation with keV-range noble gas ions followed by heating of the target and monitoring of the gas release with a mass spectrometer.

Later on, it turned out that helium atoms can be used as a probe when studying point defects in metals. Based on this fact, a new experimental method called Thermal Helium Desorption Spectroscopy (THDS) has been developed by Erents and Carter [**9**] and by Kornelsen [**5,10**]. This method consists of three steps [**11,12**]:

- a perfect, well annealed single crystal is bombarded with keV-range heavy ions to create point defects
- the defects created by irradiation are decorated with helium injected with a sub-threshold energy
- finally, the sample is heated, usually with a constant heating rate, and the desorbing helium atoms are monitored by a mass spectrometer

If the mobility of defects is of interest, the sample can be annealed to an appropriate temperature after heavy ion bombardment. After each desorption cycle the sample can be annealed such that the same sample can be used in further experiments. The method described above is also called helium-probing technique (HPT) [**13**]. The steps of a THDS cycle are presented in Fig. 1.1.

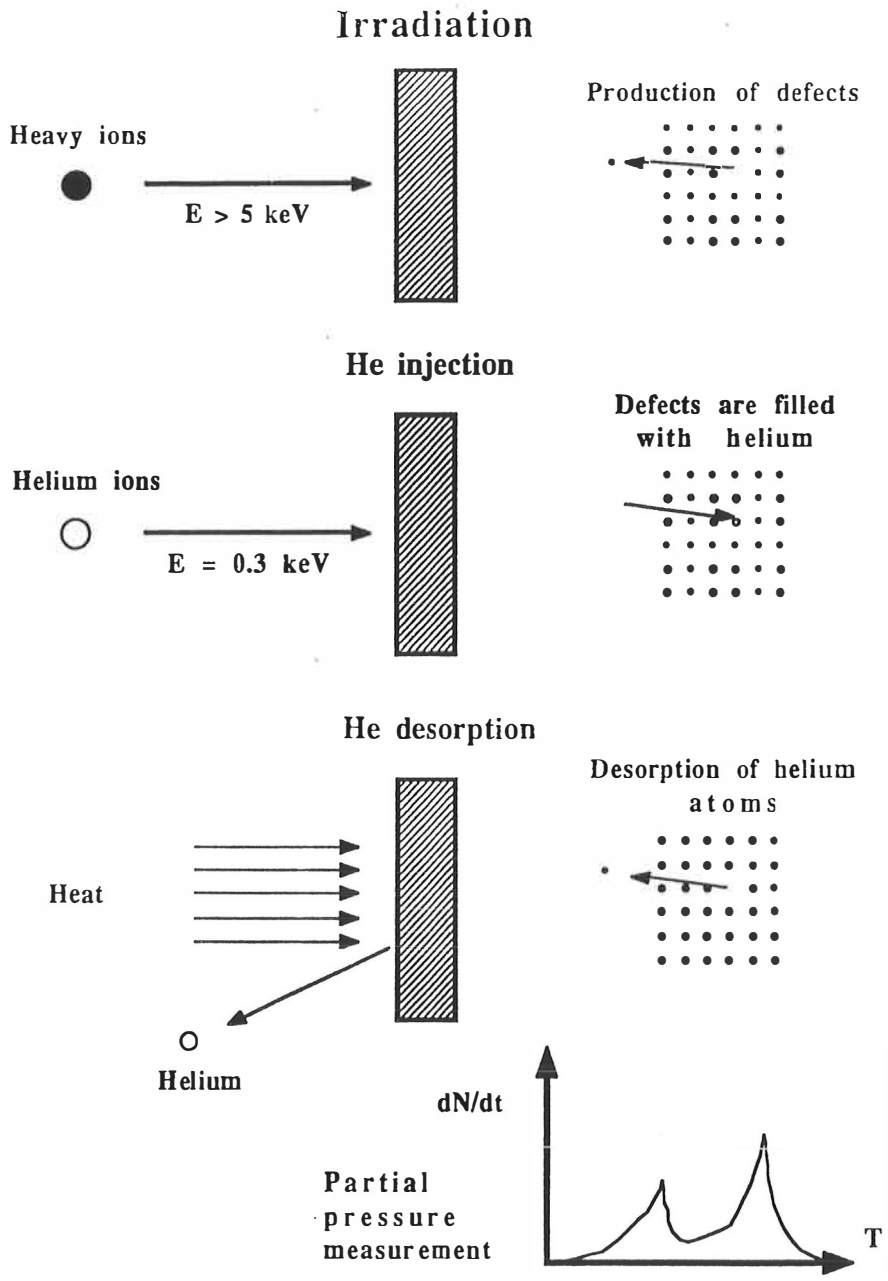

Figure 1.1. *Principle of a THDS procedure when probing point defects.*

There are several physical properties that make helium a suitable probe atom [9,10]. Helium atoms are light and they have a high thermal speed. Because of a low activation energy for interstitial motion, helium is practically insoluble in perfect metals and highly

mobile at room temperature. Furthermore, helium is strongly trapped by open-volume defects such as vacancies and vacancy clusters. The dissociation energy in such defects is of the order of a few electron volts, which is essentially higher than the binding energies of rare gases on outer surface. This implies that the helium release observed in THDS experiments comes most probably from inside the crystal and not from the surface. From the experimental point of view helium has an advantage of being a minor component of the residual gas in vacuum systems; it is easy to create a vacuum system with a negligible helium background.

By analysing a THDS spectrum the kinetic parameters such as the dissociation energy, the rate constant and the reaction order can be obtained. The number of desorbing atoms can also be determined. Since most of the helium atoms are released from an open-volume defect filled with one helium atom, a reasonable measure for the concentration of defects can be obtained. However, a fraction of the desorbing helium atoms are released from multiply filled defects, and an accurate determination of the vacancy concentration is usually very complicated.

Although the principle of the THDS method is rather simple, there are many experimental difficulties that make it very challenging. The main difficulties arise from the detection of small amounts of gas, typically 10^{10} - 10^{13} atoms during a THDS experiment. Moreover, due to a limited penetration of keV-range ions, the crystals to be investigated have to be clean with a well defined surface. Therefore the THDS experiments have to be made in ultra-high vacuum conditions. There may also be some other difficulties to be faced when applying this method to different metals; the assumptions concerning the properties of helium are not always valid.

The experimental solid state group at the Department of Physics, University of Jyväskylä, has concentrated on investigating radiation damages in solids created by ion beams [**14,15**]. So far the investigations have been carried out by utilizing the positron-lifetime method [**16**] and the positron-lifetime spectrometer constructed in Jyväskylä [**17**]. To get a more comprehensive view on these phenomena, a project to construct a THDS facility was launched in 1989. This thesis is a review of the development and test period of the facility. Some attention has been paid to the theory of desorption kinetics, as well as on the analysing methods associated with thermal desorption experiments. The rest of the thesis is dedicated to experimental results, dealing with the behaviour of noble gases in copper according to the preliminary desorption measurements.

2. Desorption kinetics

2.1. First-order kinetics

Thermal desorption spectra are usually described by first-order kinetics, and hence the desorption rate can be expressed as [**18,19**]

$$\frac{dN}{dt} = -\nu_0 N \exp(-E_D/k_B T), \tag{2.1.}$$

where N is the number of desorbing particles in the crystal, dN/dt is the desorption rate, ν_0 is the rate constant, E_D is the dissociation energy (activation energy) associated with the defect, k_B is the Boltzmann constant and T is the absolute temperature. Eq. (2.1.) is based on a classical treatment of a particle in a potential well (depth E_D). Consider that the potential can be approximated as a harmonic potential well and ν_0 is the characteristic frequency of the particle. Each particle makes ν_0 jumps per unit time. Assuming that N is large, $N(t)\exp(-E_D/k_B T)$ gives the number of particles with $E \geq E_D$, which is needed to escape from the potential well. The rate constant is usually assumed to be independent of temperature.

The analysis of first-order kinetics becomes essentially easier, if the sample is heated with a constant heating rate, that is $dT/dt = \mu$. Substituting this in Eq. (2.1.) one obtains

$$\frac{dN}{dT} = -\frac{\nu_0}{\mu} N \exp(-E_D/k_B T). \tag{2.2.}$$

At the peak temperature T_P, which corresponds to the maximum of the intensity, the second derivative with respect to temperature is zero, which results in the equation

$$\frac{\nu_0}{\mu} \exp(-E_D/k_B T_P) = \frac{E_D}{k_B T_P^2}. \tag{2.3.}$$

The peak temperature can thus be determined, if E_D, ν_0 and μ are known.

Eq. (2.2.) is a differential equation which can be approximately solved by partial integration:

$$N(T) = N_0 \exp\left\{ -\frac{\nu_0}{\mu} \exp(-E_D/k_B T) T \sum_{n=1}^{\infty} (-1)^{n+1} (n)! \left(\frac{k_B T}{E_D} \right)^n \right\}. \qquad (2.4.)$$

Here N_0 is the initial number of desorbing particles. The sum appearing in Eq. (2.3.) does not converge. However, since the term $(k_B T/E_D)$ is usually very small (at the peak temperature $(k_B T_P/E_D) \approx 0.03$), the first terms of the series tend to converge. After a straightforward calculation it can be proved that

$$\frac{dN}{dT} = -\frac{\nu_0}{\mu} N \exp(-E_D/k_B T)\,(1 + \xi_{m+1})\,. \qquad (2.5.)$$

The residual term ξ_{m+1} corresponds to the systematic error made by taking into account the first m terms in the diverging sum. The absolute value of the residual term is bound by

$$|\xi_{m+1}| \leq (m+1)! \left(\frac{k_B T}{E_D} \right)^m$$

The FWHM of a first-order desorption peak is usually less than 10 % of the peak temperature. Therefore the essential shape of the peak can be determined when $0.025 \leq k_B T/E_D \leq 0.050$. Assuming that m=10 and $k_B T/E_D = 0.050$ the error is found to be

$$\xi_{11} \leq 11!(0.05)^{10} \approx 4 \cdot 10^{-6},$$

which gives a reasonable accuracy for calculating theoretical peaks.

An alternative approach for solving Eq. (2.2.) is to utilize the incomplete gamma-functions [**20,21**]. After separating the variables we get

$$\begin{aligned}
\int_{N_0}^{N(T)} \frac{dN}{N} &= -\frac{\nu_0}{\mu} \int_0^T \exp(-E_D/k_B t)dt \\
&= -\frac{\nu_0 E_D}{\mu k_B} \int_{E_D/k_B T}^{\infty} \frac{\exp(-u)}{u^2} du \\
&= -\frac{\nu_0 T}{\mu} \int_1^{\infty} \frac{\exp(-E_D v/k_B T)}{v^2} dv \\
&= -\frac{\nu_0}{\mu} T E_2\left(\frac{E_D}{k_B T}\right),
\end{aligned}$$

where $E_2(x)$ is, by definition, the incomplete gamma function of the second kind. Using the recursion relation E_2 can be expressed by E_1:

$$E_2(x) = \exp(-x) - xE_1(x) = \exp(-x)(1 - R(x)),$$

where $R(x)$ is a rational function associated with the incomplete gamma function of the first kind. Various approximations for $R(x)$ has been calculated in mathematical literature [**20**]. For the best approximations, the absolute error in $R(x)$ is of the order of 10^{-8}.

Using the gamma function formalism, $N(T)$ and its temperature derivative can be written as

$$\begin{aligned}
N(T) &= N_0 \exp\left\{-\frac{\nu_0 T}{\mu} \exp(-E_D/k_B T)\left[1 - R\left(\frac{E_D}{k_B T}\right)\right]\right\}, \\
\frac{dN(T)}{dT} &= -\frac{\nu_0}{\mu} N_0 \exp\left\{-\frac{\nu_0 T}{\mu} \exp(-E_D/k_B T)\left[1 - R\left(\frac{E_D}{k_B T}\right)\right] - \frac{E_D}{k_B T}\right\}.
\end{aligned} \tag{2.6.}$$

The incomplete gamma function formalism gives, in principle, an accurate method to evaluate the desorption rate. In practice, due to the limited accuracy in estimating $R(x)$, this method is not essentially better than the series expansion appearing in Eq. (2.4.).

What are the characteristic features of the first-order kinetics, then? Firstly, the peak in the desorption-rate curve is asymmetric with respect to the peak temperature, as illustrated in Fig. 2.1. Secondly, the FWHM of the peak is roughly 7 - 10 % of the peak temperature, depending on the rate constant associated with the reaction. Thirdly, the peak temperature is independent of the initial number of desorbing particles. Therefore

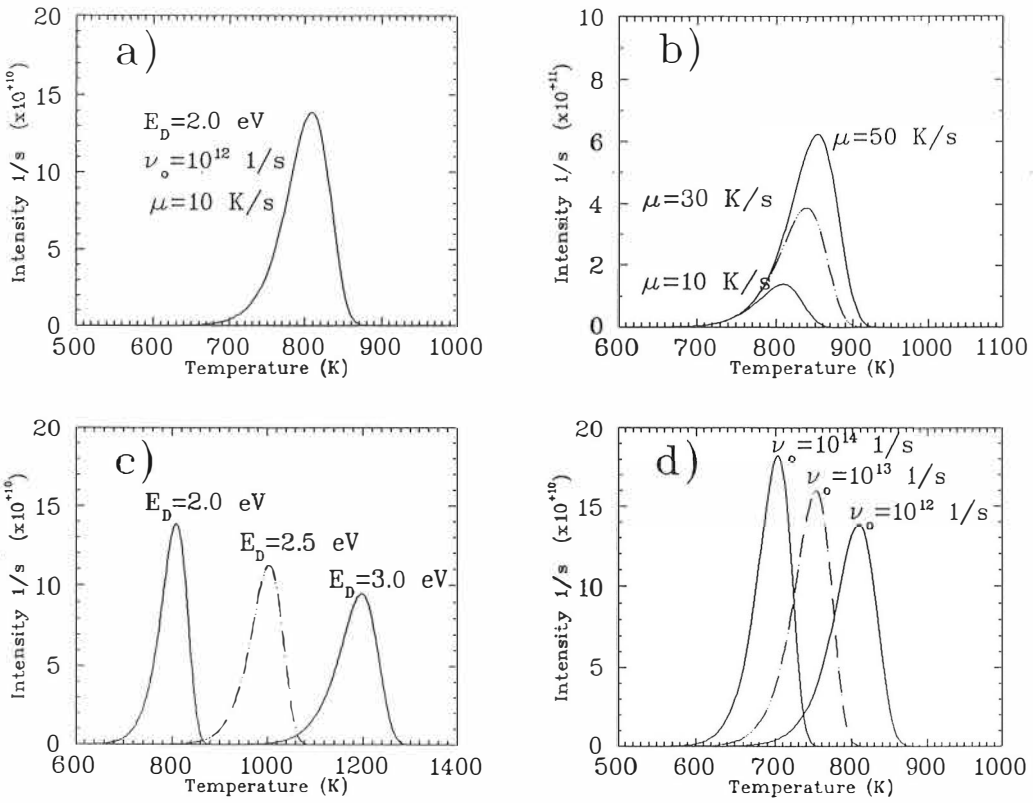

Figure 2.1. *Some features of first-order desorption spectra. a) A typical shape of a theoretical first- order spectrum calculated with the parameters indicated in the figure. b) The peak temperature as well as the desorption rate increases when using higher heating rates. c) When the activation energy increases, the corresponding peak is observed at a somewhat higher temperature. d) If the rate constant increases, the peak shifts towards lower temperatures.*

the peak temperature does not depend on the implantation dose. Finally, the peak temperature is also independent of the implantation energy, i.e. the diffusion time to escape at the surface is negligible. Some typical trends of first-order kinetics are shown in Fig. 2.1. The spectra appearing in Fig. 2.1. are calculated assuming that $E_{\mathrm{D}} = 2.0$ eV, $\nu_0 = 10^{12}$ 1/s and $\mu = 10$ K/s, if not otherwise specified.

2.2. Higher-order kinetics

A general, n^{th} order kinetics, can be defined as

$$\frac{dN}{dt} = -\nu_0 N^{\text{n}} \exp(-E_{\text{D}}/k_{\text{B}}T), \tag{2.6.}$$

that is, the time derivative of the number of particles is proportional to N^n, where n is an arbitrary integer. Similarly to the first-order case, an analytic expression for the desorption rate can be derived.

Second-order kinetics has usually little to do with noble gas release from solid crystals. The phenomena in which second-order behaviour is observed are usually associated with collision processes on surfaces. For example, the probability that two identical atoms collide with each other is proportional to the square of the particle concentration [**22**].

2.3. Diffusion

When using first-order kinetics to describe THDS phenomena, the particles are treated as if they were instantly observable in vacuum after their release from a defect. This implies that the diffusion process through the crystal has to be extremely rapid, i.e. the time to migrate a few tens of atomic layers is negligible and the change in temperature during this time interval is much less than the width of the first-order kinetic peaks.

When a helium atom starts its random walk inside a metal lattice, it feels a periodic potential energy when travelling from one interstitial site to another. The periodic potential is illustrated in Fig. 2.2.

When no defects are present, a helium atom has to overcome a potential barrier called the migration energy E_{M}. In the case of vacancies, the binding energy E_{B} is the net depth of a trap, and the dissociation energy E_{D} is the total depth of a vacancy-type trap. The dissociation energy, which is the quantity measured in the THDS experiments, is usually expressed as a sum of the migration energy and the binding energy, that is

$$E_{\text{D}} = E_{\text{M}} + E_{\text{B}}. \tag{2.7.}$$

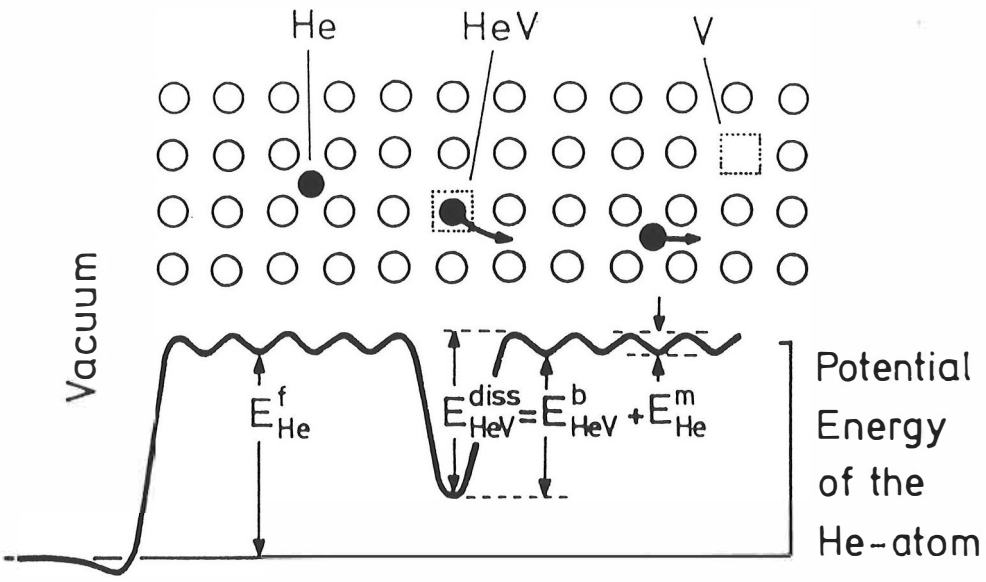

Figure 2.2. *Potential energy of a helium atom at different lattice sites in metals [23].*

However, there are also some deviations from this simple formula, mainly because the periodicity of the crystal is evidently distorted by crystal relaxation in the vicinity of a vacancy.

The high mobility of helium is essential for the THDS method. On one hand, the vacancies created in a crystal can not be filled with helium, if helium atoms can not move by interstitial migration. On the other hand, when measuring the spectra the diffusion steps should be as rapid as possible such that the desorption rate is mainly controlled by a single-step release from a point defect. This means that the migration energy has to be clearly smaller than the dissociation energy of a helium-vacancy pair. Moreover, the migration energy has to be low enough such that the injected helium atoms are essentially free in the temperature in which the ion bombardments of a THDS experiment are made. At the same time the vacancies have to remain immobile.

The migration energies of helium for different metals have been usually estimated by theoretical calculations [**24-31**]. The results tend to vary depending on which kind of helium-metal interactions are used in the calculations. Some values of theoretical migration energies for helium in different metals are collected in Table 2.1. Detailed descriptions of the behaviour of gas implants in metals can be found in Refs. [**32,33**].

Table 2.1. *Some theoretical values for the migration energy of helium in different metals.*

Metal	*BCC/ FCC*	E_M *(eV)*	*Reference*
W	BCC	0.24	[24]
Mo	BCC	0.23	[24]
Ta	BCC	0.00	[24]
V	BCC	0.13	[24]
Al	FCC	0.33	[29]
Cu	FCC	0.63	[29]
Ni	FCC	0.66	[29]
Ag	FCC	0.65	[29]
Au	FCC	0.72	[29]

The migration energies for helium in FCC metals seem to be essentially higher than the ones in BCC metals. The deviation may result from the differences in symmetry: the interstitial positions in a FCC crystal are more separated. However, the results are evidently rather sensitive to the helium-metal interaction used in the calculations. There are still a limited amount of experimental data concerning the migration energy of helium in different metals [**34-41**], and in some cases the interpretations can be criticized [**35-37, 40**]. In general, the migration energy is essentially smaller than the dissociation energy of helium in a vacancy. Since the desorption rate, as well as the diffusion rate, depend exponentially on the corresponding energy parameter, the diffusion time is negligible and the process is controlled mainly by the jump mechanism from a vacancy.

The gas release, controlled by successive jumps from one interstitial site to another, can not be described by first-order kinetics alone. In such a case, the desorption model should be modified as follows. Firstly, let us define the relaxation time for diffusive motion as

$$\tau_D = \frac{\exp(E_M/k_B T)}{\nu_0}, \tag{2.8.}$$

to describe the average time for one succesful jump. If a gas atom starts its random walk n atomic layers beneath the surface, the number of jumps it needs to escape from the surface is n^2, because the diffusion time is proportional to the square of the diffusion length. Hence

$$\tau_{D,n} = n^2 \cdot \frac{\exp(E_M/k_B T)}{\nu_0} \equiv \frac{\exp(E_M/k_B T)}{\nu_{Eff}}, \qquad \nu_{Eff} = \frac{\nu_0}{n^2}. \tag{2.9.}$$

According to Eq. (2.9.) the delay due to diffusion can be taken into account by replacing the initial rate constant with a term ν_0/n^2. Eq. (2.9.) has to be applied to each atomic layer inside the implantation profile.

A more sophisticated way to study the migration of interstitial impurities is based on the diffusion equation

$$\frac{\partial c(r,t)}{\partial t} = D\nabla^2 c(r,t), \tag{2.10.}$$

where $c(r,t)$ is the impurity concentration and D is the diffusion coefficient. The diffusion coefficient for such a process can be defined as [**42,43**]

$$D = \frac{2}{3}\lambda^2 \nu_0 \exp(S/k_B)\exp(-E_M/k_B T), \tag{2.11.}$$

where λ is the distance between two atomic layers, ν_0 is the frequency of characteristic oscillations of the impurity in the periodic potential and S is the entropy of the oscillating impurity. Since the temperature dependence of entropy in the case of a system of harmonic oscillators is relatively weak [**44**], the term $\exp(S/k_B)$ can be regarded as a constant, and the diffusion coefficient can be written as

$$D = \frac{2}{3}\lambda^2 \nu \exp(-E_M/k_B T). \tag{2.12.}$$

When the diffusion equation is applied to describe the thermal release of impurities from a solid crystal, the fact that the diffusion coefficient depends on temperature has to be taken into account. Moreover, the imposed boundary conditions of the solutions of Eq. (2.10.) have to correspond to the appropriate physical conditions.

Assuming that the impurity profile is a gaussian distribution with an average depth of d and with a standard deviation of σ, a simple model can be created. If the sample is heated with a constant heating rate, the time dependence of D can be evaluated. Since the general diffusion problem can be reduced to one dimension, the solution of Eq. (2.10.) can be written as

$$c(x,t) = \frac{c_0}{\left\{4\int D\,(T(t))\,dt + \sigma^2\right\}^{\frac{1}{2}}} \exp\left\{\frac{-x^2}{4\int D\,(T(t))\,dt + \sigma^2}\right\}. \tag{2.13.}$$

The impurity release is proportional to the particle-current density $j(x,t)$ at $x = d$, which, according to Fick's law, can be written as [**45**]

$$j(d,t) = -D\frac{\partial c(d,t)}{\partial x} = \frac{2dc_0D}{\left\{4\int D\,(T(t))\,dt + \sigma^2\right\}^{\frac{3}{2}}} \exp\left\{\frac{-d^2}{4\int D\,(T(t))\,dt + \sigma^2}\right\}. \quad (2.14.)$$

Some typical features of the model described by Eq. (2.14.) are presented in Fig. 2.3. The default parameters used in the simulations are $E_M = 0.50$ eV, $\nu = 10^{13}$ 1/s, $\mu =$ 1.0 K/s, and $d = 100$ atomic layers, if not otherwise specified. Here d is the depth of the initial gaussian distribution with a standard deviation of 50 %. It should be noted that if a gas-release process is controlled by diffusion only, the shape of the spectrum differs from that of the first-order kinetics.

The model for diffusive release seems to be rather reasonable to describe e.g. the effect due to different implantation profiles. In general, the behaviour of diffusive release is rather similar to that of first-order kinetics, with the exception that the effects due to different penetration of different ions become visible. The peak temperature satisfies Eq. (2.3.) if the factor ν is replaced by ν/n^2. Thus our crude model, expressed in Eq. (2.9.), is in accordance with the model derived from the diffusion equation. Moreover, the peak temperature of an intensity distribution due to diffusive release seems to be quite insensitive to the standard deviation of the implantation profile.

The diffusion model described above might be a useful tool to determine the migration energy directly by monitoring the gas release as a function of temperature. Since the model is based on some simplifying assumptions it does not necessarily describe properly a real physical system in which lattice relaxation and anharmonic effects have to be taken into account. The model also assumes that the interstitial mechanism is the only mechanism for diffusion.

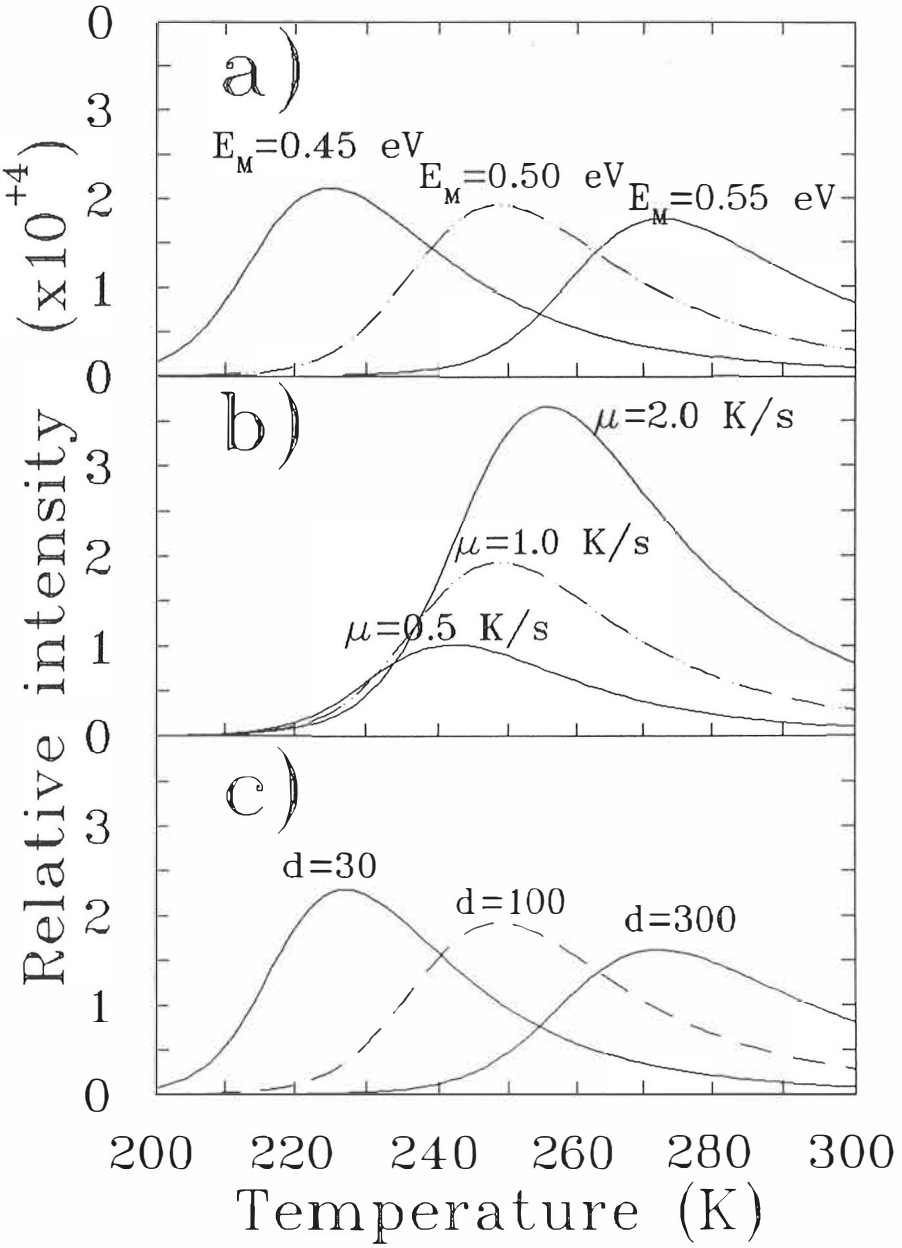

Figure 2.3. *Simulated diffusion spectra a) with different migration energies, b) with different heating rates, and c) with different implantation depths, calculated according to Eq. (2.14.).*

3. On the analysis of first-order kinetics

When the analysis of thermal desorption spectra is based on first-order kinetics, each peak can be described with three parameters: the dissociation energy E_D, the rate constant ν_0 and the initial number of particles N_0. There are plenty of methods to obtain these parameters from experimental data [**46-54**]. In this chapter some of these methods are discussed from the experimental point of view, when the signals are always rather weak containing noise and when the background differs from zero.

3.1. Variation of the heating rate

According to first-order kinetics, the peak temperature depends on the heating rate of the sample. This means that to each heating rate μ_i, there corresponds a peak temperature T_{P_i}. Eq. (2.3.) is valid for every heating rate - peak temperature pair. If the same experiment is carried out with two heating rates, μ_1 and μ_2, they correspond to two peak maxima T_1 and T_2, respectively. Using Eq. (2.3.) the dissociation energy for desorption can be expressed as

$$E_D = \frac{k_B T_1 T_2}{T_1 - T_2} \ln\left(\frac{\mu_1 T_2^2}{\mu_2 T_1^2}\right), \tag{3.1.}$$

since E_D does not depend on the heating rate. Once the dissociation energy has been determined, the rate constant can be calculated from Eq. (2.3.). The initial number of particles N_0 can be obtained by integration, i.e.

$$N_0 = \int \frac{dN}{dt} dt. \tag{3.2.}$$

Usually the initial number of particles is not of great importance, especially in the case of the first-order kinetics, since it only affects the absolute intensity but not the temperature dependence.

When the same experiment is repeated with several heating rates, a more reliable analysis can be obtained. Eq. (2.3.) can also be expressed as [**46**]

$$\ln(\frac{T_P^2}{\mu}) = \frac{E_D}{k_B}\frac{1}{T_P} + \ln(\frac{E_D}{k_B \nu_0}) \equiv a_1 \frac{1}{T_P} + a_0, \qquad (3.3.)$$

that is, if the terms $\ln(\frac{T_{P_i}^2}{\mu_i})$ are plotted as a function of $(1/T_{P_i})$, a linear dependence is obtained. The parameters E_D and ν_0, as well as their error limits, can be easily determined just by making a standard least-squares fit.

An example of the shift of the maximum of a desorption peak is presented in Table 3.1. The peak temperatures are obtained as numerical solutions of Eq. (2.3.) when the dissociation energy $E_D = 2.0$ eV and the rate constant $\nu_0 = 1.0 \cdot 10^{13}$ 1/s.

Table 3.1. *Theoretical peak temperatures when using different heating rates.*

μ [K/s]	T_P [K]	$1/T_P$ [1/K]	$LN(T_P^2/\mu)$
1.0	702.8	$1.4228 \cdot 10^{-3}$	13.110
2.0	717.0	$1.3947 \cdot 10^{-3}$	12.457
3.0	725.6	$1.3781 \cdot 10^{-3}$	12.075
4.0	731.8	$1.3665 \cdot 10^{-3}$	11.804
5.0	736.7	$1.3574 \cdot 10^{-3}$	11.594
6.0	740.7	$1.3501 \cdot 10^{-3}$	11.423
7.0	744.2	$1.3437 \cdot 10^{-3}$	11.279
8.0	747.2	$1.3383 \cdot 10^{-3}$	11.153
9.0	749.8	$1.3337 \cdot 10^{-3}$	11.042
10.0	752.2	$1.3294 \cdot 10^{-3}$	10.943

Changes in the heating rate affect relatively little the position of the peak (T_P increases about 2 %, when the heating rate is increased by a factor of two). However, this effect is very sensitive to systematic errors caused by the increasing heating rates. The error may be due to a slight delay in the response of the temperature measurement system, or due to temperature gradient in the sample. This effect is demonstrated in Fig. 3.1., where the data of Table 3.1. is plotted. As seen in the figure the theoretically calculated data suggest a perfect linear dependence (solid circles and solid line) according to Eq. (3.3.). The situation is totally different, if a systematic error exists. In Fig. 3.1. the systematic error is expected to be directly proportional to the heating rate, that is

$$T_P' = T_P - \tau_T \cdot \mu, \qquad (3.4.)$$

where T_P' is the measured temperature, T_P is the real temperature and τ_T is a time constant characteristic of the temperature measurement system. As illustrated in Fig. 3.1., the analysis becomes nearly impossible, if the time constant is of the order of one second. As a result, the activation energy tends to increase very rapidly, and the data points do not form a perfect linear fit any more.

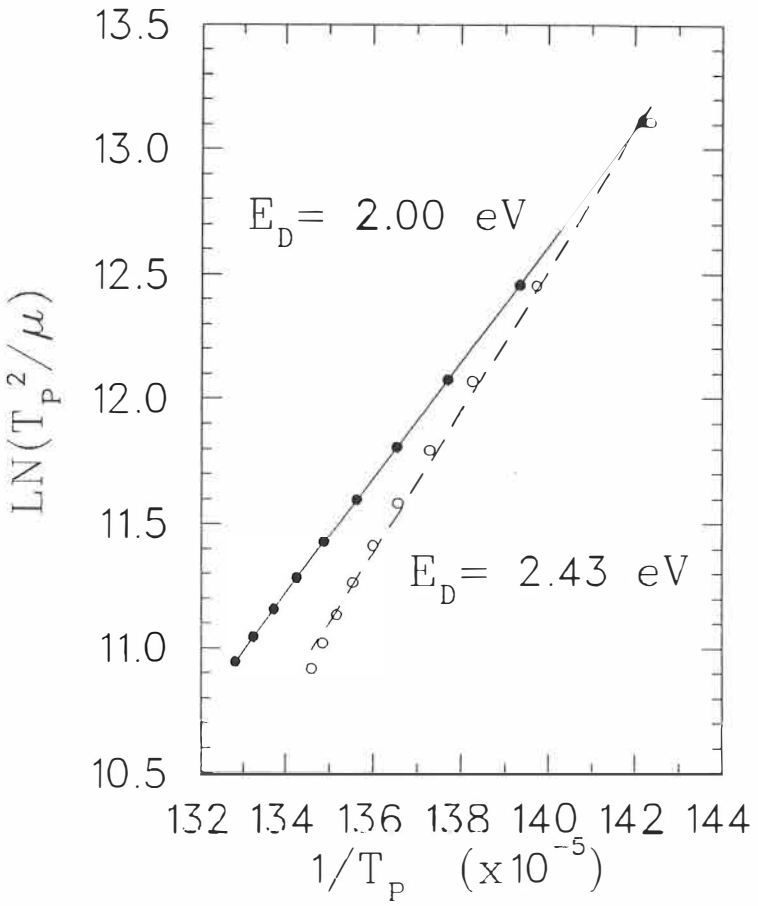

Figure 3.1. *The effect of systematic errors in temperature measurement. The data expressed in Table 3.1. (solid circles) give a perfect Arrhenius plot (solid line) and the correct activation energy of* 2.00 eV *can be obtained. If the temperature measurement system is perturbed by a delay of one second, a totally different behaviour (open circles) is obtained.*

The delay described above may be caused by the time constant of a thermocouple, which is widely used in temperature measurements when performing thermal desorption experi-

ments. The peak shift may also be distorted by the limited accuracy of the thermocouple. Therefore, if the analysis is based on the variation of the heating rate, the possibility of systematic errors should be taken into account. For the same reason, very high heating rates (several tens of degrees kelvin per second) may result in large errors when determining the activation energy. A sufficient peak shift can also be obtained with very slow heating rates, provided that the signal can be distinguished from the background.

3.2. Peak-area analysis

Since there is always some problems to determine the peak temperature from experimental data, some methods have been developed to minimize the effects of the noise in the measurements. These methods utilize the integrated area of the peak, which according to Eq. (3.1.) corresponds to the number of desorbing particles in the sample.

Suppose that we have a desorption spectrum that obeys first-order kinetics. The desorption rate can be expressed as

$$R(T) = -\frac{dN}{dt} = \nu_0 N(T) \exp(-E_D/k_B T). \tag{3.5.}$$

Let us choose two temperatures T_1 and T_2, such that $T_1 < T_P < T_2$ and $R_1 = R_2$. Since the desorption rates are equal, it follows that

$$\nu_0 N_1 (\exp(-E_D/k_B T_1) = \nu_0 N_2 \exp(-E_D/k_B T_2). \tag{3.6.}$$

Solving for E_D we obtain [**47**]

$$E_D = \frac{k_B T_1 T_2}{T_1 - T_2} \ln\left(\frac{N_2}{N_1}\right). \tag{3.7.}$$

A more general formula which is valid for n^{th} order kinetics, can be written as

$$E_D = \frac{n k_B T_1 T_2}{T_1 - T_2} \ln\left(\frac{N_2}{N_1}\right), n \geq 1. \tag{3.8.}$$

The number of desorbing particles N_i associated with each temperature T_i can be obtained by integration

$$N_i = \int_{T \geq T_i} \frac{dN}{dt} dt. \tag{3.9.}$$

The determination of N_i is presented in Fig. 3.2.

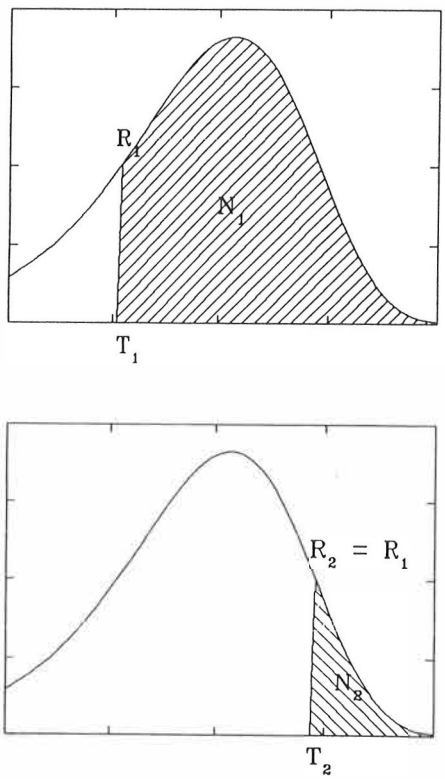

Figure 3.2. *Determination of the number of desorbing particles for two different temperatures.*

A more general expression for the determination of the activation energy can be obtained if Eq. (3.5.) is rewritten as [**48,49**]

$$\frac{R(T)}{N(T)} = \nu_0 \exp(-E_D/k_B T). \tag{3.10.}$$

Taking a logarithm one obtains

$$\ln\left(\frac{R(T)}{N(T)}\right) = -\frac{E_D}{k_B}\frac{1}{T} + \ln(\nu_0), \qquad (3.11.)$$

that is, the rate equation can be converted into a linear form as a function of 1/T. The activation energy and the rate equation can be determined by making a linear least-squares fit. The same idea has been introduced previously by van Gorkum [**50**], and the analysis is based on the characteristic time for desorption.

The methods based on the integration of the spectrum are not very sensitive to the noise in experimental data. However, some difficulties may arise when eliminating the background which usually differs from zero. The formula (3.7.) tends to yield a reasonable accuracy. On the other hand, the linearization of a desorption spectrum usually gives unreasonable results, mainly because the linear dependence can be easily distorted in the beginning and in the end of the spectrum, where the actual desorption rate can hardly be distinguished from the background.

Since the determination of the number of desorbing particles is based on integration, the peak-area methods are difficult to apply to a spectrum containing more than one peak.

3.3. Peak-width analysis

Although the analytic expression for the desorption rate is very complicated, some simple trends can be observed when investigating simulated spectra. The peak temperature increases with increasing activation energy if the rate constant and the heating rate are not changed. Moreover, the half width of a desorption peak depends on the peak temperature, i.e. the ratio $\Delta_{1/2}/T_P$ is a slowly-varying function of E_D.

Some results of simulated desorption spectra are presented in Fig. 3.3. The activation energy is varied from 1.0 eV up to 3.0 eV. The simulations were performed assuming a rate constant $\nu_0 = 1.0 \cdot 10^{13}$ 1/s and using a heating rate of 1.0 K/s. The peak temperature and the half-width of each peak were determined numerically. The accuracy in the determination of T_P and $\Delta_{1/2}$ was 0.001 K.

Since the term $T_P^2/(\Delta_{1/2} \cdot E_D)$ was found to be nearly independent of the other kinetic parameters, some further simulations were made. It turned out that if the rate constant is varied by several orders of magnitude, this term does not actually remain constant, but

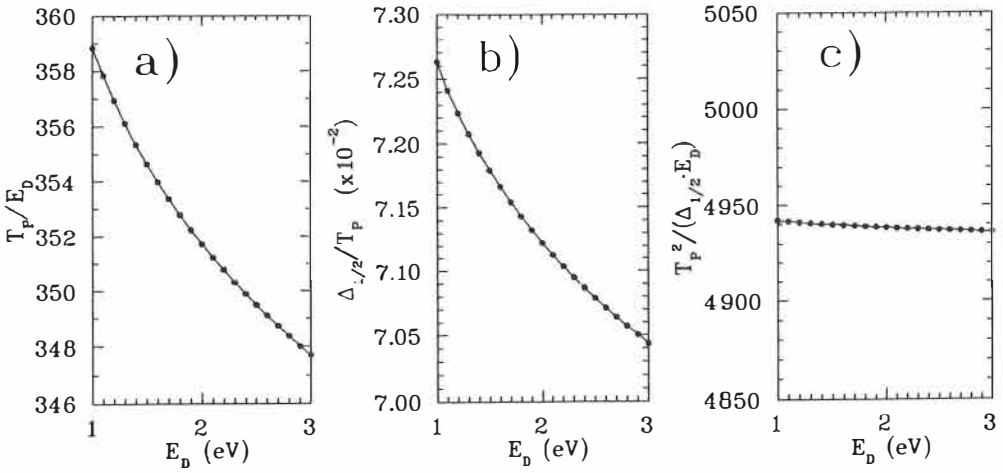

Figure 3.3. *Some general trends of simulated desorption spectra. a) The peak temperature divided by the activation energy is a slowly-varying function of* E_D. *b) The ratio* $\Delta_{1/2}/T_\mathrm{P}$ *is also nearly independent of* E_D. *c) The term* $T_\mathrm{P}^2/(\Delta \cdot E_\mathrm{D})$ *undergoes extremely small relative changes with varying* E_D.

is a smooth function that evidently can be approximated succesfully by a power series expansion. The simulation data is collected in Table 3.2. The simulations were made with an activation energy of 2.0 eV, and a heating rate of 10.0 K/s. The rate constant was varied from 10^8 1/s up to 10^{19} 1/s, comprising the vibration frequencies that usually exist in solids.

The term $T_\mathrm{P}^2/(\Delta_{1/2} \cdot E_\mathrm{D})$ tends to decrease smoothly with increasing ν_0 values. This trend is illustrated in Fig. 3.4. in which this term is plotted as a function of $T_\mathrm{P}/E_\mathrm{D}$. Since the curve in Fig. 3.4. is nearly linear it is reasonable to make a fit of the form

$$\frac{T_\mathrm{P}^2}{\Delta_{1/2} \cdot E_\mathrm{D}} = a_0 + a_1 \left(\frac{T_\mathrm{P}}{E_\mathrm{D}} \right). \qquad (3.12.)$$

The parameters can be determined using a standard least-squares method. Using the data of Table 3.2. one obtains

Table 3.2. *Some theoretical peak temperatures and half-widths of first-order peaks. The simulations were carried out with an activation energy of* 2.0 eV, *and with a heating rate of* 10.0 K/s *using various rate constants.*

ν_0 (1/s)	T_P (K)	$\Delta_{1/2}$ (K)	$\frac{T_P}{E_D}$	$\frac{\Delta_{1/2}}{T_P}$ (%)	$\frac{T_P^2}{\Delta_{1/2} \cdot E_D}$
$1.0 \cdot 10^8$	1151.09	131.027	575.54	11.3829	5056.18
$3.0 \cdot 10^8$	1096.61	119.251	548.30	10.8745	5042.09
$1.0 \cdot 10^9$	1042.32	108.038	521.16	10.3652	5027.97
$3.0 \cdot 10^9$	997.09	99.099	498.55	9.9388	5016.17
$1.0 \cdot 10^{10}$	951.68	90.492	475.84	9.5087	5004.27
$3.0 \cdot 10^{10}$	913.58	83.560	456.79	9.1464	4994.25
$1.0 \cdot 10^{11}$	875.08	76.821	437.54	8.7784	4984.09
$3.0 \cdot 10^{11}$	842.58	71.344	421.29	8.4673	4975.49
$1.0 \cdot 10^{12}$	809.55	65.976	404.77	8.1497	4966.73
$3.0 \cdot 10^{12}$	781.52	61.579	390.76	7.8794	4959.27
$1.0 \cdot 10^{13}$	752.89	57.238	376.44	7.6024	4951.63
$3.0 \cdot 10^{13}$	728.49	53.658	364.24	7.3657	4945.11
$1.0 \cdot 10^{14}$	703.45	50.101	351.72	7.1222	4938.40
$3.0 \cdot 10^{14}$	682.02	47.150	341.01	6.9133	4932.64
$1.0 \cdot 10^{15}$	659.94	44.200	329.97	6.6976	4926.70
$3.0 \cdot 10^{15}$	640.98	41.740	320.49	6.5119	4921.59
$1.0 \cdot 10^{16}$	621.39	39.269	310.69	6.3196	4916.30
$3.0 \cdot 10^{16}$	604.50	37.198	302.50	6.1536	4911.73
$1.0 \cdot 10^{17}$	586.99	35.108	293.49	5.9811	4906.99
$3.0 \cdot 10^{17}$	571.36	33.350	285.93	5.8318	4902.85
$1.0 \cdot 10^{18}$	556.12	31.567	278.06	5.6763	4898.61
$3.0 \cdot 10^{18}$	542.49	30.061	271.24	5.5413	4894.91
$1.0 \cdot 10^{19}$	528.28	28.529	264.14	5.4005	4891.04

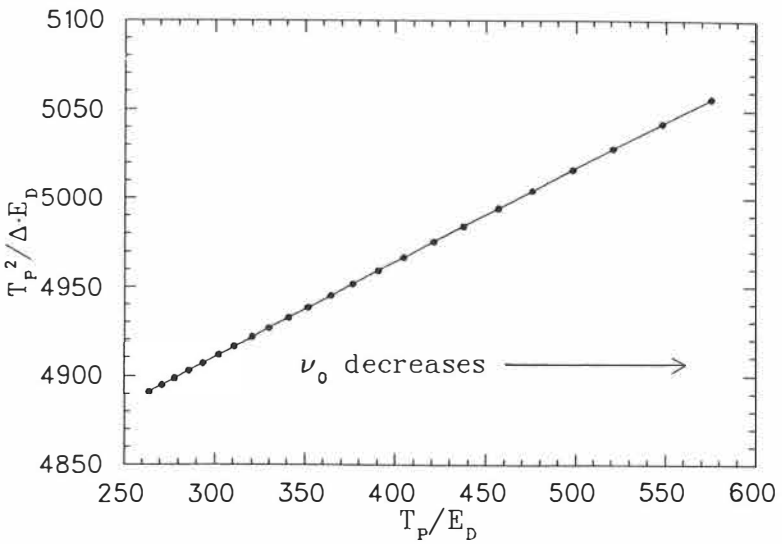

Figure 3.4. *Plot of* $T_P^2/(\Delta_{1/2} \cdot E_D)$ *vs* T_P/E_D, *based on the data presented in Table 3.2.*

$$\begin{aligned} a_0 &= 4751.2 \pm 0.4 \\ a_1 &= 0.5314 \pm 0.0009 \\ r &= 0.999945. \end{aligned} \tag{3.13.}$$

Once the parameters have been determined, an approximative analytical expression for the determination of E_D as a function of T_P and $\Delta_{1/2}$ can be derived. Solving Eq. (3.12.) for E_D and using the numerical values of Eq. (3.13.) we get

$$E_D = 2.1047 \cdot 10^{-4} \cdot \left(\frac{T_P^2}{\Delta_{1/2}} \right) - 1.1184 \cdot 10^{-4} \cdot T_P, \tag{3.14.}$$

where E_D is expressed in electron volts and the temperatures in degrees kelvin. Although the fitted expression of Eq. (3.14.) is a result of a mathematical trick and based on a limited amount of theoretically calculated first-order spectra, it was found to be valid for any activation energy, if $10^7 \leq \frac{\nu_0}{\mu} \leq 10^{18}$. The relative error in the determination of E_D was found to be of the order of 10^{-4}.

If the fit of Eq. (3.12.) is extended to include a quadratic term in T_P/E_D, and the corresponding equation is solved for E_D, the activation energy can be written as

$$E_D = \frac{\frac{T_P^2}{\Delta_{1/2}} - b_1 T_P + \sqrt{\left(\frac{T_P^2}{\Delta_{1/2}} - b_1 T_P \right)^2 - 4 b_0 b_2 T_P^2}}{2 b_0} \tag{3.15.}$$

The parameters $b_0 ... b_2$ can be determined by means of a least-squares fit yielding the values

$$\begin{aligned} b_0 &= 4743.94 \\ b_1 &= 0.569120 \\ b_2 &= -4.62482 \cdot 10^{-5}. \end{aligned} \tag{3.16.}$$

Eq. (3.15.) was tested with theoretically calculated spectra, and it yields essentially better results than Eq. (3.13.). The relative error when using Eq. (3.15.) is less than $2 \cdot 10^{-6}$ for $10^7 \leq \frac{\nu_0}{\mu} \leq 10^{18}$.

The idea of the peak-width analysis as such is not a new one. According to Chen [**51**] the activation energy for desorption can be expressed as

$$E_D = 2k_B T_P \left\{ \frac{1.26 \cdot T_P}{\Delta_{1/2}} - 1 \right\}. \tag{3.17.}$$

Edwards [**52**] has proved that the term $\Delta_{1/2}/T_P$ can be expressed as a power series of $k_B T_P/E_D$. As a result, the activation energy for desorption can be expressed as

$$E_D^F = \frac{2.4464 k_B T_P^2}{\Delta_{1/2}} \left\{ 1 - 0.5725 \left(\frac{\Delta_{1/2}}{T_P} \right) + 0.2625 \left(\frac{\Delta_{1/2}}{T_P} \right)^2 \right\}, \tag{3.18.}$$

$$E_D^S = \frac{3.5255 k_B T_P^2}{\Delta_{1/2}} \left\{ 1 - 0.5673 \left(\frac{\Delta_{1/2}}{T_P} \right) + 0.2366 \left(\frac{\Delta_{1/2}}{T_P} \right)^2 \right\}, \tag{3.19.}$$

where the indices F and S correspond to the case of first-order or second-order kinetics, respectively.

The peak-width analysis carried out by Chan et al. [**53**] is based on the determination of the desorption rate by means of the incomplete gamma functions. As a result, the formulae for the calculation of E_D can be written as

$$E_D^F = k_B T_P \left\{ \frac{-1 + T_P \sqrt{\left(\frac{\Delta_{1/2}}{T_P} \right)^2 + 5.832}}{\Delta_{1/2}} \right\}, \tag{3.20.}$$

$$E_D^S = 2k_B T_P \left\{ \frac{-1 + T_P \sqrt{\left(\frac{\Delta_{1/2}}{T_P} \right)^2 + 3.117}}{\Delta_{1/2}} \right\}. \tag{3.21.}$$

All the formulae described above give the activation energy with a reasonable accuracy, i.e. the relative error is about 10^{-4}, when compared to theoretically calculated desorption spectra. The formula presented in Eq. (3.15.) is, however, the most accurate one.

In fact, the Eqs. (3.14.), (3.15.), (3.17.) and (3.18.) reflect the same idea: the term $T_P^2/(\Delta_{1/2} \cdot E_D)$ is nearly constant, and corrections, if needed, can be obtained using any reasonable parameter such as $(k_B T_P/E_D)$ or $(\Delta_{1/2}/T_P)$. The same result can be obtained, after an elaborate calculation, by expressing the desorption rate as a Taylor series expansion at $T = T_P$.

The peak-width analysis as such is not a perfect method alone, since the exact determination of the half-width of a desorption peak is difficult because of noisy signals. However, this method gives a reasonable initial guess for the peak fitting, or a reference result when the analysis is based on the peak shift with different heating rates.

3.4. Peak fitting

Desorption spectra seldomly consist of one single first-order peak. Therefore, it should be estimated whether it is possible to determine the kinetic parameters of a spectrum with several desorption peaks which may be slightly overlapping.

The most objective method for this is to assume that the spectrums is a sum of independent first-order peaks, that is

$$\begin{aligned} R(T) &= \sum_i R_i, \\ &= \sum_i \nu_{0_i} N_{0_i}(T) \exp(-E_{\mathrm{D}_i}/k_{\mathrm{B}}T), \end{aligned} \tag{3.22.}$$

and each of the components R_i can be written in an approximate analytic form as given in Eq. (2.4.) and (2.5.). The parameters associated with each component can hence be determined by making a nonlinear least-squares fit with $3 \times n$ parameters, where n is the number of first-order peaks to be fitted in the spectrum.

A common way to make a nonlinear least-squares fit is based on an initial guess of the parameters and the values of the parameters are then iterated step by step to obtain a satisfactory result. Since the values of first-order parameters may vary within a relatively wide range, the initial guess should be determined with a great care.

If the peaks are plainly visible, the activation energy of each peak can be estimated using the peak-width analysis. Once a reasonable value for the activation energy is obtained, the rate constant can be calculated using Eq. (2.3.).

Although the number of desorbing particles associated with a certain defect is usually not of great importance, this parameter has to be determined when applying a peak-fitting procedure. If the desorption peaks are overlapping, the number of particles of each

individual defect is difficult to determine by integration. A better method for the determination of N_0 is the following. Consider that the peak temperature and the corresponding activation energy can be evaluated with a reasonable accuracy. The desorption rate at the peak temperature can be written as

$$R(T_P) = |\frac{dN(T_P)}{dt}| = \frac{N(T_P)\mu E_D}{k_B T_P^2}. \tag{3.23.}$$

Moreover, by combining Eqs. (2.3.) and (2.4.) together, the number of desorbing particles at $T = T_P$ can be written as

$$N(T_P) = N_0 \exp\left\{-1 + 2\frac{k_B T}{E_D} - 6\left(\frac{k_B T}{E_D}\right)^2 + \cdots\right\}. \tag{3.24.}$$

Hence, the initial number of desorbing particles can be estimated as

$$N_0 = \frac{R(T_P)k_B T_P^2}{\exp\left\{-1 + 2\frac{k_B T}{E_D} - 6\left(\frac{k_B T}{E_D}\right)^2 + \cdots\right\}\mu E_D}. \tag{3.25.}$$

After determining the values of the kinetic parameters for each peak, the parameter values can be made more accurate for instance by using a linear approximation instead of the complicated rate equations.

The peak-fitting method was tested and a computer program was written for making the fits. A typical result of multi-peak fitting is shown in Fig. 3.5. The parameters obtained from the fitting program are listed in Table 3.3.

Table 3.3. *Kinetic parameters associated with the calculated peaks in Fig. 3.5. The values of* N_0 are only scaling factors.

Peak	T_P (K)	E_D (eV)	ν_0 (1/s)	N_0
1	479.9	0.88	$7.23 \cdot 10^7$	$3.32 \cdot 10^{-9}$
2	533.2	1.15	$3.38 \cdot 10^9$	$3.74 \cdot 10^{-9}$
3	593.5	1.21	$7.26 \cdot 10^8$	$2.35 \cdot 10^{-9}$
4	683.8	1.92	$6.94 \cdot 10^{12}$	$4.66 \cdot 10^{-9}$

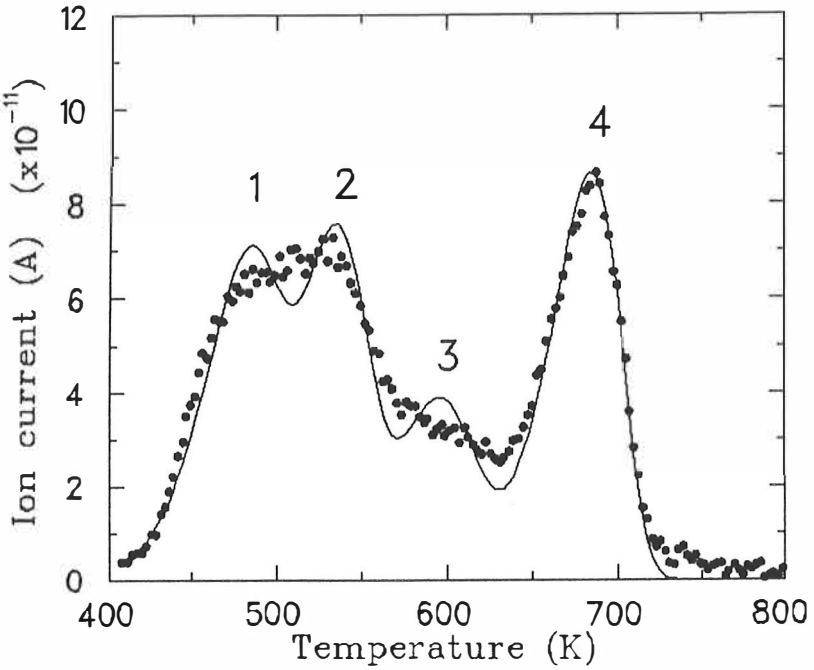

Figure 3.5. *Attempt to fit theoretically calculated first-order desorption peaks to experimental data. The experimental data ponts are marked with dots and the solid line corresponds to theoretical fit with five first-order peaks. For further information see Table 3.3.*

If the peaks appearing in an experimental spectrum are strongly overlapping, a peak-fitting procedure usually gives rather unreliable results. Especially the rate constants tend to attain unreasonable values. For instance, some of the rate constants in Table 3.3. are far too low when compared to the Debye frequences of most metals. On the other hand, the most conspicuous peak in Fig. 3.5. can be fitted with realistic values of the kinetic parameters and with a reasonable accuracy.

3.5. Comparison of the methods

The analysis of first-order kinetics is always rather difficult, mainly due to the sensitivity of the corresponding mathematical model. Since the rate constant depends exponentially on the activation energy, a small deviation in E_D results in a great deviation of ν_0. Therefore

it is not possible to get an accurate value for the rate constant. Moreover, there are many possibilities for systematic errors in the measurement, which may result in some errors in the analysis.

The method based on Arrhenius fitting is usually considered a reliable procedure [**54**]. However, as mentioned previously in this chapter, a relatively small error in the temperature measurement may distort the fitting resulting in a higher value for the activation energy. For the same reason, the corresponding rate constant obtained from such a fitting is far too large ($> 10^{15}$ Hz) to be associated with a reasonable process in a metal lattice. If the data points of the plot do not show a linear behaviour, it may be a symptom of some errors in the temperature measurement.

The peak-area method has been derived directly from the definition of first-order kinetics without any approximations. When using this method the main difficulties arise from the fact that the base line of an experimental spectrum is rather difficult to determine, especially because the background may depend slightly on temperature. Further difficulties may be encountered when applying this method to a spectrum which contains more than one peak.

The peak-width analysis usually yields reasonable results if the peaks can be clearly separated. In practice this means that the difference in temperature of two successive peaks has to be of the order of the half-width of the peaks, say, 10 per cent of the peak temperature. On the other hand, if the peaks are very close to each other the kinetic parameters can not be determined with a satisfactory accuracy.

To minimize the possibility of making mistakes when analysing the data one should always use at least two independent methods. If the results and the corresponding error limits obtained by using different analysing methods are comparable, there is hardly any doubt whether the analysis is correct.

4. Experimental facility

4.1. Technical requirements for THDS

The phenomena investigated in THDS experiments happen within a few tens of atomic layers from the surface. Therefore one of the basic requirements is to guarantee the purity of the sample. It is well-known that pure metal surfaces can be investigated only in ultra-high vacuum (UHV) conditions. Since the number of desorbing helium atoms is usually very small, say, at most 10^{13} atoms [**55**], it is necessary to minimize the helium background.

The samples used in THDS experiments are usually less than 1 cm in diameter with a thickness of 1 - 2 mm [**55**]. During the experiments the sample has to be heated up to 1000 K or higher, depending on the material investigated. Usually the sample is heated with a constant heating rate of 1 - 50 K/s. Therefore a computer-controlled heating system is needed.

The desorbing atoms are detected with a mass spectrometer which has to be capable of detecting weak and noisy signals. Moreover, at least one ion source is needed for implantations. In some cases, there are two ion sources installed in the facility, one tuned for delivering low-energy helium ions and the other for producing keV-range ion beams.

Generally, the instrumentation of a helium desorption facility is always very complicated, and there are only few descriptions in literature concerning the technical details [**55-57**].

4.2. Vacuum system

THDS measurements are usually carried out in ultra-high vacuum conditions with a total pressure of 10^{-8} Pa when the partial pressure of helium is about 10^{-10} Pa. Since there is a demand for minimizing the helium background, the problem can not be solved by using ion pumps or other gettering pumps. On the other hand, helium is also rather difficult to deal with kinetic pumps such as diffusion pumps or turbomolecular pumps, mainly because of a high thermal speed of helium atoms.

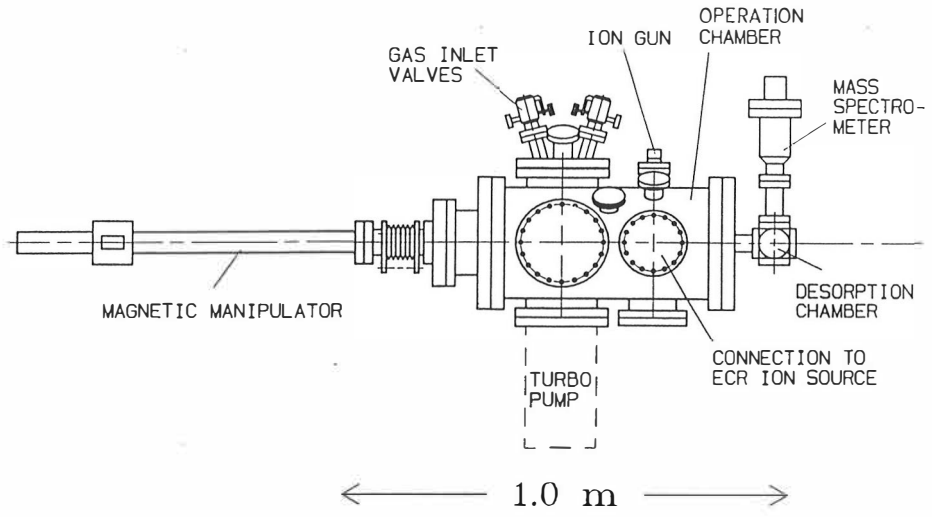

Figure 4.1. *Vacuum system of the THDS facility [58].*

Based on the experiences of van Veen [**57**], a turbomolecular pump was adopted as a main pump of the vacuum system. The vacuum system consists of an UHV chamber with a volume of 35 ℓ, pumped by a turbomolecular pump (Varian Turbo-V 450). A scheme of the vacuum system is shown in Fig. 4.1. The ports are provided with ConFlat flanges with copper gaskets, and all the components are UHV compatible and they can be baked at 200 ^{o}C.

Due to the turbomolecular pump, the baking temperature of the vacuum chamber is limited to about 150 ^{o}C, while the maximum temperature in the flange of the turbomolecular pump is about 70 ^{o}C. After baking for 24 hours at 150 ^{o}C, a base pressure of $1{\cdot}10^{-8}$ Pa can be attained. The residual gas analysis (RGA) presented in Fig. 4.2. reflects a clean ultra-high vacuum system. Hydrogen (mass numbers 1 and 2) is the main component of the residual gas. Small amount of water vapour (mass number 18) is still present, evidently because of a limited baking temperature. Since the compression ratio of a turbomolecular pump is extremely high for heavy molecules, there are no hydrocarbons present.

In spite of the difficulties associated with turbomolecular pumps to process light gases, the pumping system has turned out to be effective enough to pump hydrogen and helium. The partial pressure of helium, measured by a quadrupole mass spectrometer, was found to be less than 10^{-10} Pa. Hence there is no need to improve the system for instance by combining a diffusion pump and a turbomolecular pump in series [**57**] or by using a high throughput version of a turbomolecular pump [**59**].

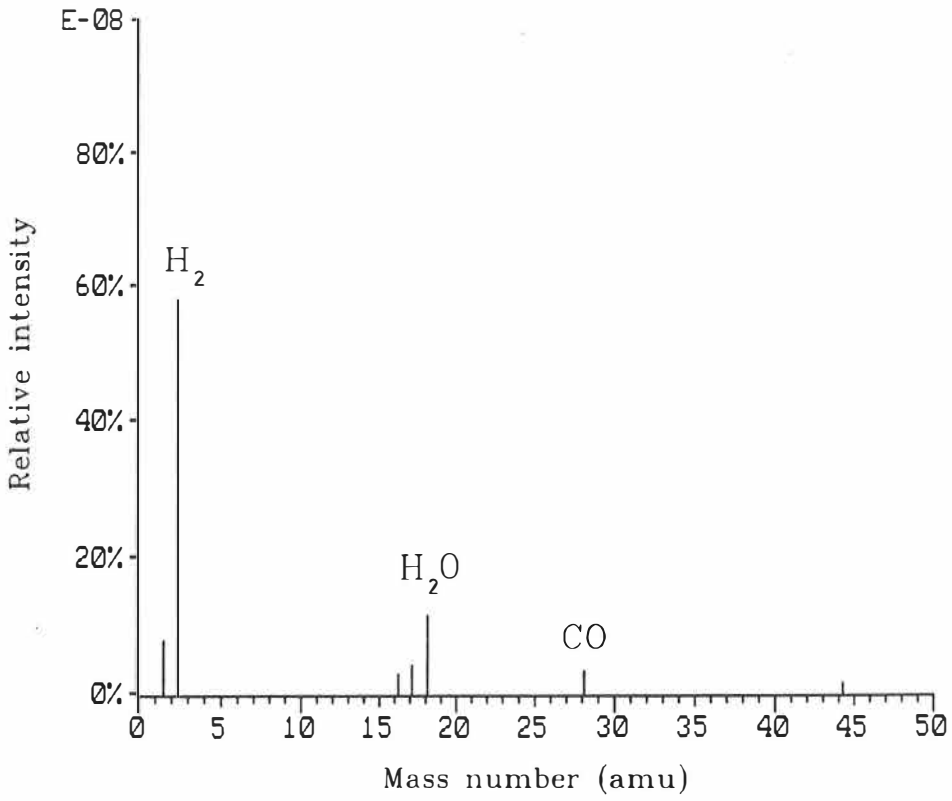

Figure 4.2. *Residual gas analysis of the desorption facility. Hydrogen is the dominating component of the residual gas.*

4.3. He detection

The helium desorption rate, derived from the equation of state for an ideal gas, can be expressed by

$$\frac{dN}{dt} = \frac{V}{k_B T}\left(\frac{dP}{dt} + \frac{P}{\tau}\right), \tag{4.1.}$$

where V is the volume of the desorption chamber, P is the measured partial pressure and $\tau = V/S$ is the pumping time constant of the desorption chamber, k_B is the Boltzmann factor and T is the ambient temperature.

The two terms appearing in Eq. (4.1.) describe the *static* and the *dynamic* modes of operation, respectively. The static mode is valid when the pumping time constant is

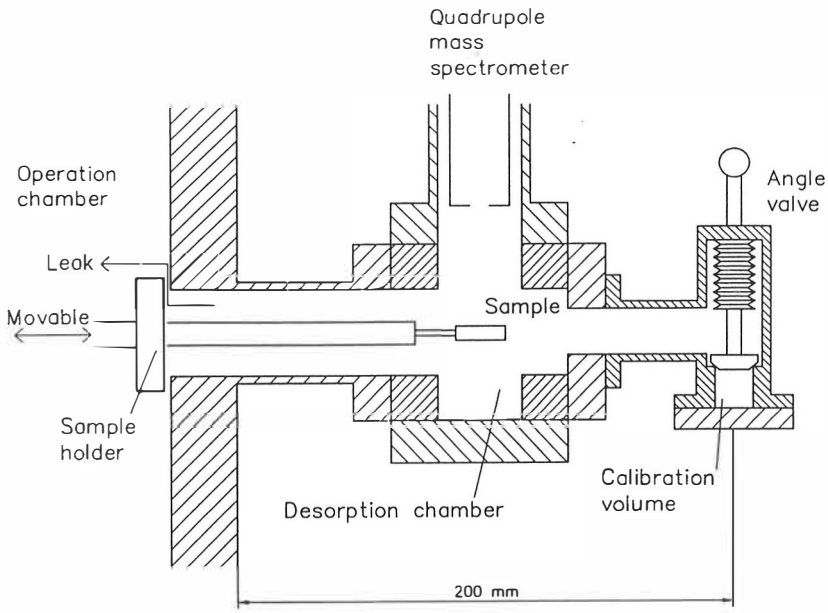

Figure 4.3. *Schematic drawing of the desorption chamber [58].*

very large, that is, the pumping speed is negligible. Alternatively, when the term $\frac{P}{\tau}$ is dominating, the system operates in the dynamic mode.

When operating in the static mode some difficulties can not be avoided. Firstly, the measurement may be interfered by residual gas occupation, since the control volume is not pumped. Secondly, the sensitivity is usually weak at the end of the heating cycle, because the noise level is proportional to $\sqrt{N}$, where N corresponds to the total number of helium atoms in the desorption volume. This may result in the disappearance of small desorption peaks [**57**]. Finally, a mass spectrometer which is used for helium detection has always a slight pumping effect and the conditions are seldom entirely static. Taking into account these facts, the dynamic operation mode is usually preferred, especially when high doses are used. In both cases it is convenient to make the desorption volume as small as possible.

The mass spectrometer (Balzers QMG 420 C) was provided with a Channeltron-type multiplier to improve the sensitivity and the collection speed. The measuring frequency is 2 - 3 measurements per second, which is a satisfactory collection speed for THDS [**55**].

To minimize the desorption volume, the sample can be transferred to a small chamber (V = 300 cm^3). The quadrupole analyzer is mounted to the same chamber. The connection of the analyzer is shown in Fig. 4.3.

The mass spectrometer can be controlled by an external PC computer using a commercial software QUADSTAR 3. The data can be stored in the computer and the measurements can be monitored and visualized utilizing the graphics of PC computers. The scheme of the mass spectrometer is shown in Fig. 4.4.

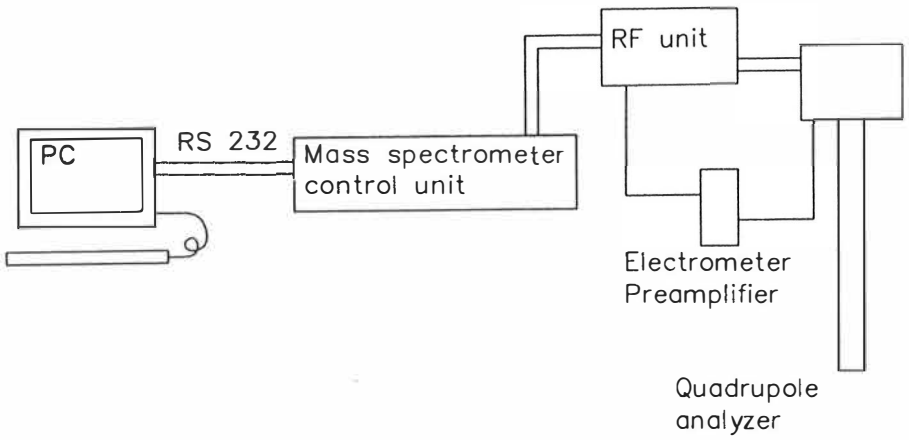

Figure 4.4. *Block diagram of the mass spectrometer installed in the THDS facility.*

The helium detection system was tested carefully to determine the pumping time constant as well as to guarantee that the system operates in the dynamic mode. The determination of the pumping time constant is based on the assumption that noble gases obey exponential pumping. Hence, the ion current measured by the mass spectrometer can be expressed by

$$I = I_0 \exp(-t/\tau) + I_b, \tag{4.2.}$$

with I_b being the background signal. The time response was measured by feeding a gas pulse to the mass spectrometer. The pumping time constant was found to be 0.1 s (see Fig. 4.5.).

Once the pumping time constant has been determined, the magnitude of the static and dynamic term can be estimated. Assuming that the ion current of the mass spectrometer is directly proportional to the partial pressure of helium, Eq. (4.1.) can be rewritten as

$$\frac{dN}{dt} \propto \left(\frac{dI}{dt} + \frac{I}{\tau}\right), \tag{4.3.}$$

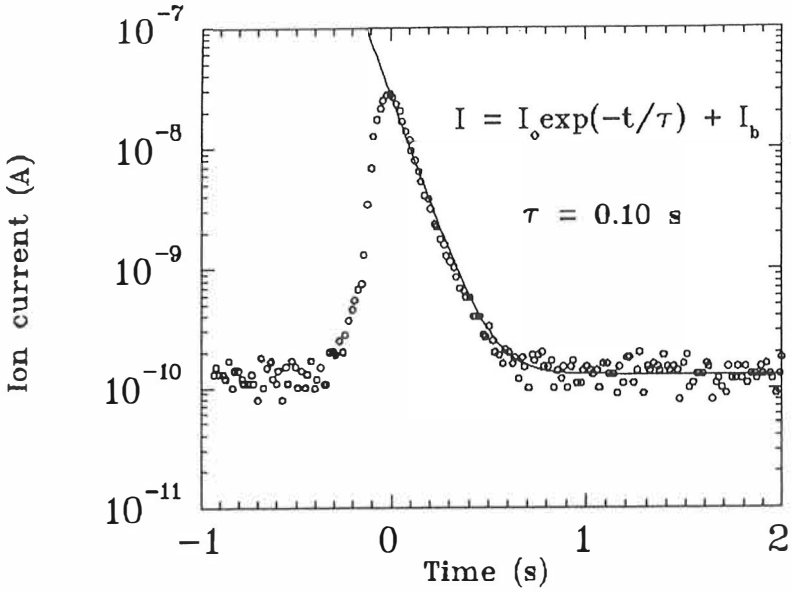

Figure 4.5. *The time response of the mass spectrometer (open circles) for a helium pulse [58]. The solid line corresponds to exponential pumping assuming that* $\tau = 0.1$ s.

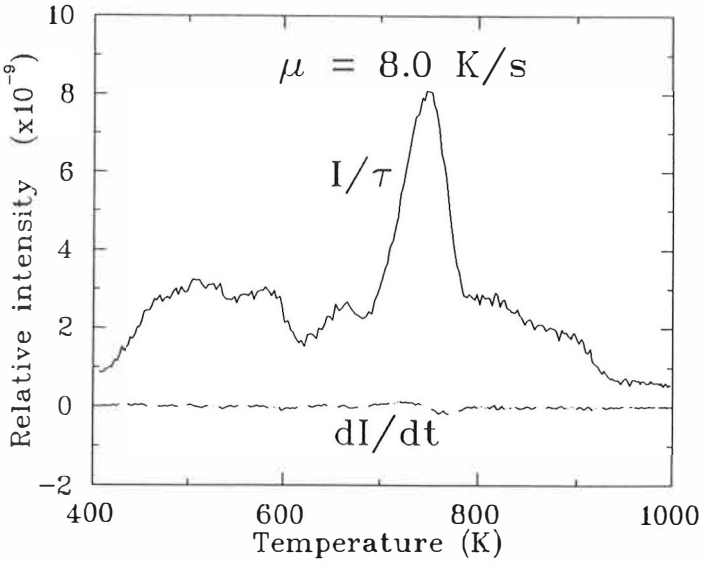

Figure 4.6. *Comparison of the dynamic term* I/τ *(solid line) and the static term* dI/dt *(dashed line) [58].*

where I is the ion current of the mass spectrometer. These two terms are illustrated in

Fig. 4.6. during a helium desorption experiment for Cu. The dynamic term (I/τ) is dominating while the static one (dI/dt) is essentially zero. We may conclude that the helium detection system operates in the dynamic mode. Moreover, the desorption rate is directly proportional to the ion current of the mass spectrometer and there is no need to make any correction in order to take into account the static term.

In some experiments, the absolute desorption rate as well as the number of desorbing atoms may be of interest. It is also necessary to check the sensitivity of the mass spectrometer frequently, since it may alter as a function of time. The helium-detection system can be calibrated by injecting a small amount of helium gas from the cavity of the small angle valve mounted to the desorption chamber. So far the pressure of the captured gas can be measured by a hot cathode ionization gauge only, and hence the accuracy of the calibration system is limited by the accuracy of the vacuum gauge [**58**]. However, it should be emphasized that in many cases reasonable information can be obtained just by measuring the temperature dependence of the relative intensity.

4.4. Sample heating and cooling

The sample heating process in THDS experiments can be approximatively expressed as

$$\begin{aligned} P_{\mathrm{Tot}} &= c\frac{dT}{dt} + P_{\mathrm{Cond}} + P_{\mathrm{Rad}} \\ &= c\mu + \alpha(T - T_{\mathrm{o}}) + \beta(T^4 - T_{\mathrm{o}}^4), \end{aligned} \tag{4.4.}$$

where P_{Tot} is the total heating power, P_{Cond} is the loss due to thermal conductivity, P_{Rad} is the power lost by thermal radiation, c is the heat capacity of the sample, T is the temperature of the sample and T_{o} is the ambient temperature. The constants α and β depend on the geometry of the sample and on the construction of the sample holder.

The heating power needed in THDS experiments depends drastically on the temperature scale used in the experiments. When the maximum operating temperature is about 1000 K, the total power consumption is usually less than 50 W, provided that the size of the sample is about 1 cm^2. When higher temperatures are used, the need of power may be essentially higher because of the dominating role of thermal radiation. Therefore, when the method is applied for example to refractory materials, the size of the sample has to be reduced to limit the heating power consumption.

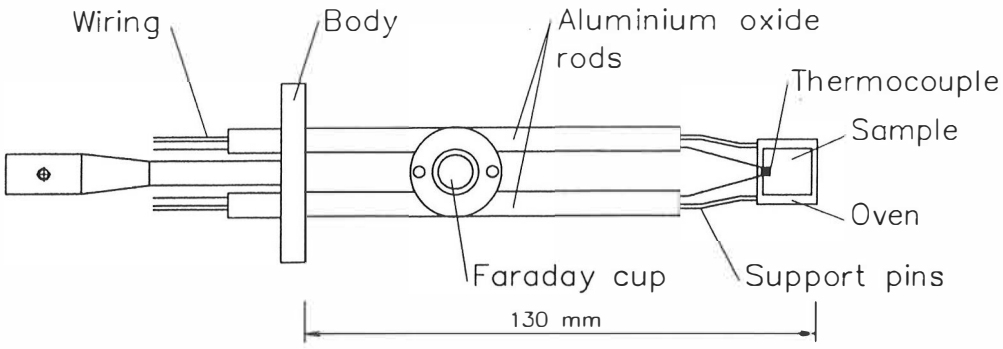

Figure 4.7. *Scheme of the sample holder [58].*

The sample can be heated using an electron gun, laser or resistive heating. Usually the sample is heated by electron bombardment onto its rear face to avoid temperature gradient in the sample [**55**]. However, we have adopted resistive heating which has turned out to be a simple and reliable solution. When using this method, there is no need to keep the sample at high potential with respect to the ground, which is necessary when using electron guns [**57**].

In THDS experiments the temperature of the sample is measured by a thermocouple or an optical pyrometer. A pyrometer is an ideal instrument to measure surface temperatures, provided that the temperatures to be measured are relatively high. However, if the measurements are started at room temperature or below, a thermocouple is the only reasonable way to measure the temperature of the sample. Since our facility contains also a sample cooling option, the temperature of the sample is measured by a K-type (Chromel - Alumel) thermocouple.

The construction of the sample holder is shown in Fig. 4.7. The sample is heated by a tungsten filament embedded in a boron nitride oven. Boron nitride has the advantage of having a low thermal expansion coefficient and a rather good thermal conductivity. Therefore such a material tolerates rapid heating cycles characteristic of THDS experiments.

The heating system as a whole consists of a PID control unit (Eurotherm 818 P), a power supply and the sample holder including the heating filament and the thermocouple junction. A scheme of the heating system is shown in Fig. 4.8. The temperature-control system is rather versatile and it has been used also for other short-term experiments [**60**].

Since the PID unit is controlled by a microprocessor, the thermoelectric voltage of most thermocouples can directly be converted to a temperature scale.

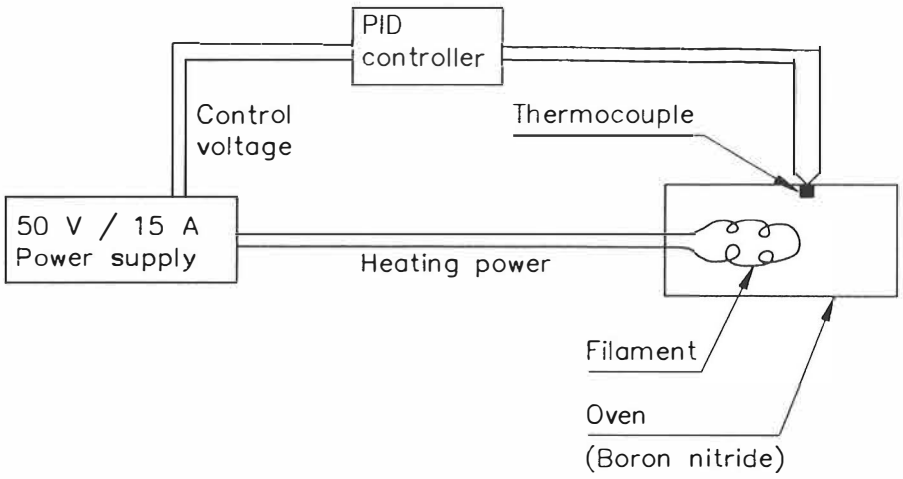

Figure 4.8. *Scheme of the temperature-control system of the THDS facility.*

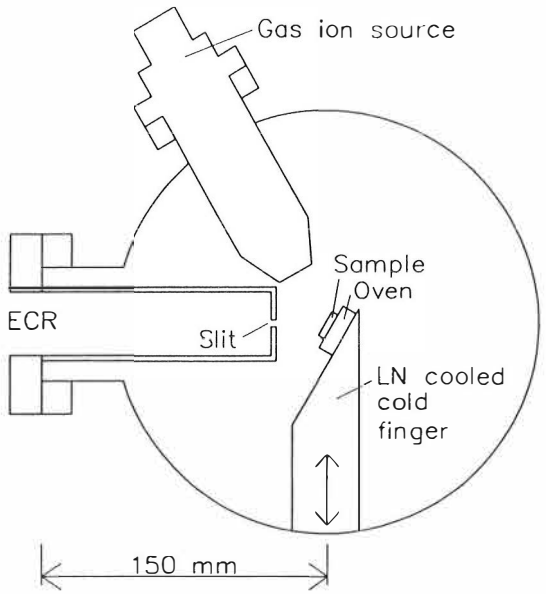

Figure 4.9. *Irradiation geometry when performing THDS experiments at low temperatures [58].*

When vacancy-type defects are studied by means of THDS, the irradiations have to be

performed below the stage III, i.e. below the temperature where monovacancies become mobile. For many metals, this temperature region exists at around 200 K [**61**]. This means that in many cases the sample has to be cooled below room temperature.

The cooling option is a contradictory demand for the construction of the sample holder, because during the cooling procedure the sample should have a good thermal contact to the environment. As illustrated in Fig. 4.9., this problem was solved by touching the sample package with a movable cold finger filled with liquid nitrogen. The minimum attainable temperature is 150 K, and it is mainly limited by the thermal load through the support pins.

4.5. Ion sources

Since the energy range of ion beams needed in THDS experiments is relatively wide, two ion sources were installed in the facility: a gas ion source for helium injections and another ion source for delivering heavy ion beams.

The beam currents needed in the experiments are a few tens of nanoamperes, which means that the irradiation time to get a dose of 10^{13} atoms is about one minute. Higher intensities may result in great deviations in determining the dose, because the irradiation time becomes very short. On the other hand, more intensive argon beams are frequently needed for sample preparation, since the surface of the sample has to be sputtered before starting the measurements.

The helium injections are produced by a sputtering ion source delivered by Varian Associates, Inc. The instrument utilizes electron-impact principle and it can be used also for producing other noble gas ions. The energy of the beams can be varied from 100 eV up to 3.0 keV.

The gas ion source is not differentially pumped and it has no mass analysis either. Therefore it is possible that the beam contains some impurities and also multiply-charged ions. These details are not expected to play an essential role in the first-principle measurements reported in this work.

The helium desorption facility utilizes the electron cyclotron resonance (ECR) ion source of the Accelerator Laboratory of the University of Jyväskylä [**62**]. The beam lines of

the JYFL-ECRIS has been constructed such that the beam of the ion source can be easily transported to the THDS facility for instance when the cyclotron is shut down for service. When the LIISA project (LIght Ion Source Apparatus) is completed, various light-ion beams for the cyclotron can also be delivered by another external ion source, which increases the use of the ECR ion source for other purposes.

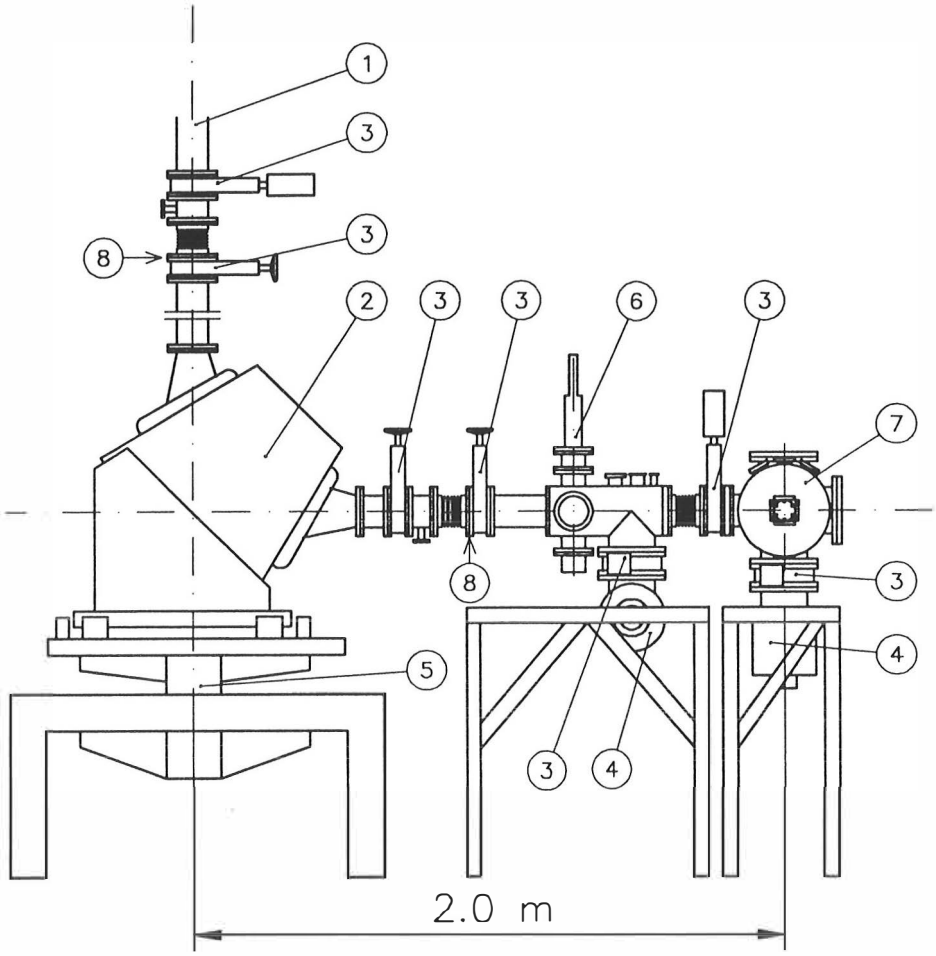

Figure 4.10. *Connection of the JYFL-ECRIS and the THDS facility [58]. 1. Vertical ECR beam line, 2. Analysing magnet, 3. Gate valve, 4. Turbomolecular pump, 5. Rotatable stand of the analysing magnet, 6. Beam diagnostics, 7. THDS facility, 8. Flanges that have to be detached when connecting the analysing magnet to the cyclotron or to the THDS facility.*

The ECR option makes it possible to use various elements for implantations. Since the

Table 4.1. *Some parameters of the ECR beams used in THDS experiments.* I_{D1} *and* I_{S1} *correspond to the currents of the analysing magnet and the first solenoid of the beam line, respectively.* I_{FC3} *corresponds to the beam current measured in the THDS facility.*

Ion	E(keV)	U(kV)	I_{D1}(A)	I_{S1}(A)	I_{FC3}(nA)
$^{3}He^{+}$	3.0	3.0	21.00	52.16	20
$^{3}He^{+}$	5.0	5.0	27.11	47.94	40
$^{3}He^{+}$	10.0	10.0	38.45	67.26	60
$^{4}He^{+}$	3.0	3.0	24.20	50.80	20-100
$^{4}He^{+}$	5.0	5.0	31.17	50.00	20-100
$^{4}He^{+}$	10.0	10.0	44.60	48.50	20-100
$^{20}Ne^{+}$	5.0	5.0	70.20	129.66	60
$^{20}Ne^{2+}$	10.0	10.0	49.48	96.37	60
$^{40}Ar^{2+}$	5.0	2.5	49.82	81.60	20-100
$^{40}Ar^{2+}$	10.0	5.0	69.99	119.00	20-100
$^{40}Ar^{4+}$	20.0	10.0	49.21	63.56	20-100
$^{40}Ar^{3+}$	30.0	10.0	81.60	120.00	20-100
$^{40}Ar^{5+}$	50.0	10.0	62.40	99.10	20-100
$^{40}Ar^{6+}$	60.0	10.0	57.70	68.50	20-100

maximum acceleration voltage of the ion source is 30 kV and the charge stages are usually very high (Ar^{10+}, for example), the beam energies available from the ECR ion source cover the energy range from a few keV up to several hundreds of keV. Since the ECR ion source can be used also for producing ions of metals and other solids [**63**], it is a unique tool for investigating implantation effects in solids.

The beam of the JYFL-ECRIS is mass-analysed by a 90^{o} dipole magnet which is also used for separating different charge stages. The beam is transported to the desorption facility through a differential pumping section such that the pressure level of the ECR beam lines ($\sim 10^{-5}$ Pa) is reduced about three orders of magnitude. The differential pumping section is separated by slits that act also as collimators. In spite of the rather simple arrangement, the pressure of the desorption facility can be kept in the 10^{-8} Pa level when irradiating the sample with the ECR ion source. The analysing magnet and the differential pumping section are shown in Fig. 4.10.

A choice of the ECR beams used so far in the THDS experiments is presented in Table 4.1. When heavy-ion beams are needed, the charge state of the ions has to be considered in such a way that a sufficient intensity can be attained. Moreover, since the magnetic rigidity of the analysing magnet is limited to about 0.17 T·m, it is convenient to use as high q/m ratios as possible.

4.6. Sample preparation

The samples (purity 99.999 %) used in these experiments were delivered by the Metal Laboratory of Outokumpu Copper, Inc. The surface was finished by mechanical polishing followed by electrolytical polishing procedure. Before mounting the sample in the sample holder some micrographs were taken by an atomic force microscopy (AFM) indicating that the quality of the surface was satisfactory. The orientation of the crystal was not specified. Before starting the measurements, the surface was sputtered with argon to remove some tens of atomic layers. Finally, the sample was annealed several times at 1000 K to get rid of argon impurities.

The facility itself has not any instrument to be used for checking the purity and the orientation of the crystal, which can be regarded as a severe problem. In the case of copper, the quality of the surface was found to be changed after a few desorption experiments. This was expected due to contamination by impurities or due to deformation of the surface during repeated heating cycles to elevated temperatures. Actually, there is both experimental [**64-66**] and theoretical [**67**] evidence that some anomalous phenomena take place when dealing with copper surfaces at high temperatures.

5. Helium in copper

5.1. Energy-dose dependence

To get a reasonable picture on the behaviour of helium in copper, a systematic series of experiments was performed by bombarding a copper single crystal with He beam using different energies and doses. The irradiations were made at room temperature, and the energy range covered from 0.1 keV up to 10 keV, while the doses were varied from 10^{12} to 10^{14} ions/cm^2. The bombarding geometry was chosen according to Fig. 4.9., i.e. the angle of the beam was 30° with respect to the normal of the surface.

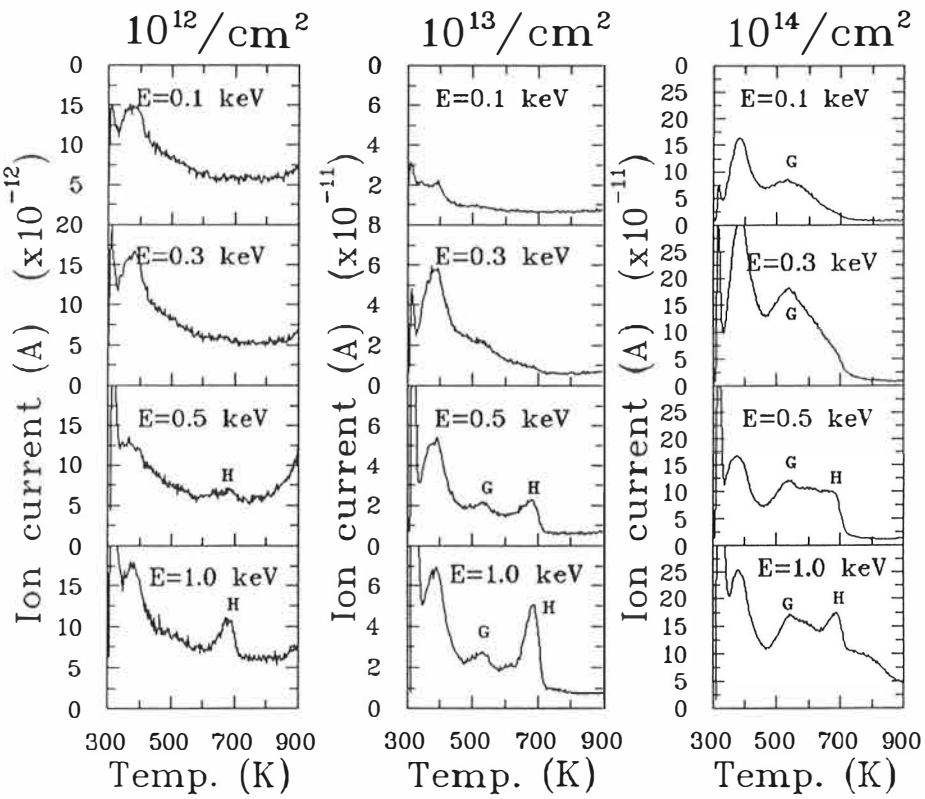

Figure 5.1. *Helium desorption spectra of Cu irradiated with low helium energies.*

A summary of the experiments carried out with bombardment energies ≤ 1 keV is pre-

sented in Fig. 5.1. The irradiations were made using the gas ion source of the facility. The helium release in each spectrum was measured with the mass spectrometer while heating the sample from 300 K up to 900 K with a heating rate of 1.0 K/s. The peaks are marked using the systematics of Buters et al. [68]. The interpretation of each peak is discussed in more detail in chapter 5.2.

When the bombarding energy is a few hundreds of electron volts, no clear first-order peaks can be observed. At around 0.5 keV, the peak marked with H is observed, which evidently can be associated with helium release from monovacancies. The same peak is clearly observed with the bombarding energy of 1.0 keV, and at the same time another distribution, called the G peak, can be seen at around 540 K.

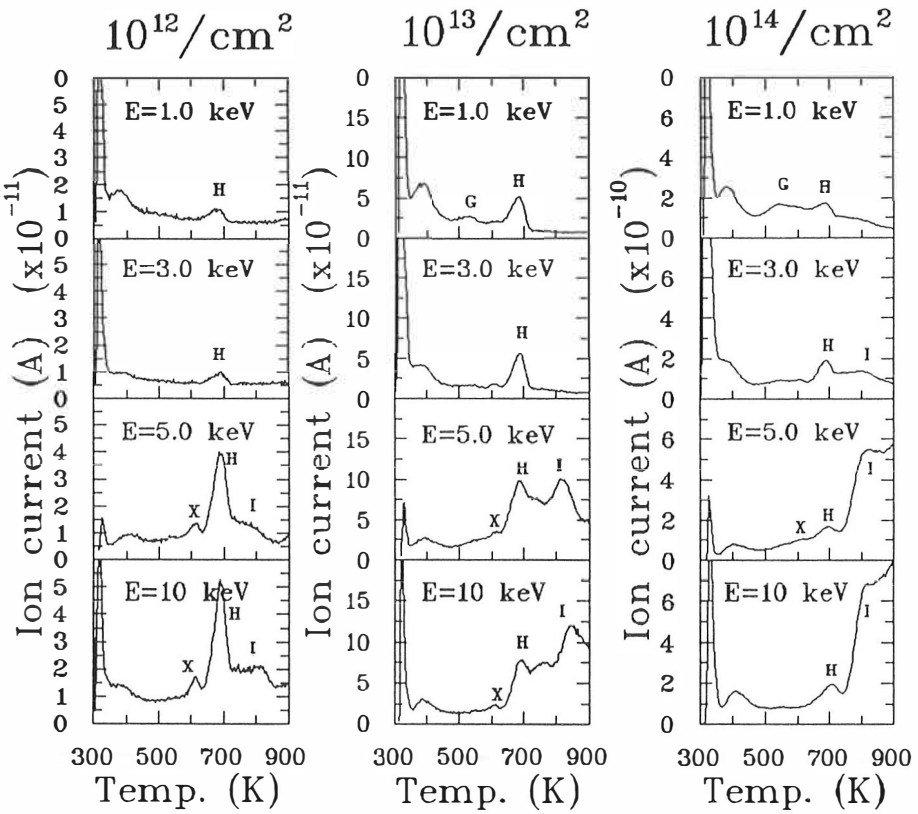

Figure 5.2. *Helium desorption spectra when using keV-range bombarding energies.*

The peaks described above are well separated when using a dose of 10^{13} ions/cm^2. When this dose level is exceeded, the intensity of the G peak increases remarkably with respect to the vacancy peak, and the peaks can hardly be distinguished with each other.

When the bombarding energy is several keV, the shape of the H peak can be clearly observed when using low implantation doses (see Fig. 5.2.). The intensity tends to increase with increasing bombarding energies. This may be due to the fact that the scattering from the first surface layer decreases when using higher energies. Moreover, when the implantation energy is increased, more vacancies per helium atom can be produced, and the probability of being trapped increases.

The G peak seems to disappear with higher bombarding energies, or, it is replaced by another peak (the X peak) which appears at around 600 K. The interpretation of this replacement is discussed in chapter 5.2.

A general trend concerning the spectra related to keV-range bombarding energies is the fact that a new distribution is observed at relatively high temperatures ($T \geq 800$ K). This effect seems to be enhanced with increasing bombarding energy. Another feature of this so called I peak is that its intensity, as compared to that of the H peak, grows when using higher doses.

5.2. Characterization of the peaks

According to the measurements described elsewhere [**68,69**] the H peak can be associated with helium release from monovacancies. This interpretation is supported by the energy dependence. To yield this peak visible, a threshold energy of a few hundreds of electron volts is needed. The observation is roughly in agreement with the one estimated from the energy transfer in an elastic head-on collision. In such a case, the kinetic energy transferred to a recoil atom can be expressed as

$$E_{\mathrm{k}} = \frac{4m_1m_2}{(m_1+m_2)^2}E_o. \qquad (5.1.)$$

To create a vacancy, the energy transferred to a recoil has to exceed a value called the displacement threshold energy E_{d}, which is the minimum energy to create a Frenkel pair, i.e. a vacancy-interstitial pair [**70**]. The accurate values of E_{d} depend on the metal concerned and also on the direction of the colliding atom with respect to the lattice orientation. The lattice atom that receives the kinetic energy directly from a colliding ion is called the primary knock-on atom (PKA).

Usually the actual value of E_d is replaced by an average value E_d^{avg}, which is roughly independent of the orientation of the crystal. The values of E_d^{avg} are of the order of 25 eV, clearly higher than the minimum energy to create a Frenkel pair.

Eq. (5.1.) gives the maximum kinetic energy transferred to a recoil atom. In practice, the collisions resulting in lower energies for recoils are more probable. The number of defects produced by a PKA can be estimated using the cascade theory formulated by Kinchin and Pease [**71**]. According to the theory, the number of Frenkel pairs produced by a recoil with an energy of E_k is

$$n = \frac{0.8E_k^*}{2E_d^{avg}}, \tag{5.2.}$$

where E_k^* is an effective value of the kinetic energy of the recoil which takes into account the losses due to electronic exitations, and n is the number of Frenkel pairs produced.

The average displacement threshold energy for copper is 29 eV [**70**]. In the case of helium and copper, one can estimate that the average minimum energy of a helium ion to create one Frenkel pair is 150 eV. It is fully another thing whether the colliding ion is trapped by the vacancy created by itself. However, a clear indication of a first-order distribution can be observed in Fig. 5.1. when the bombarding energy exceeds 500 eV. This implies that the H peak can be associated with helium release from monovacancies.

The dose dependence of the H peak is relatively weak which means that the probability to create such a defect is at most directly proportional to the dose. This indicates that there is only one helium atom inside the defect. We may thus assume that the helium release associated with the H peak can be described by

$$HeV \rightarrow He + V. \tag{5.3.}$$

The character of the G peak can be concluded directly from Fig. 5.3. The intensity of the G peak increases rapidly when the dose level exceeds 10^{13}/ cm^2. The effect is clearly visible when using bombarding energies of about 1 keV. This means that the trapping rate associated with the G peak is strongly dependent on the helium dose. On the other hand, the G peak disappears when using bombarding energies of several keV. Combining these facts together one can deduce that the G peak represents multiply-filled monovacancies.

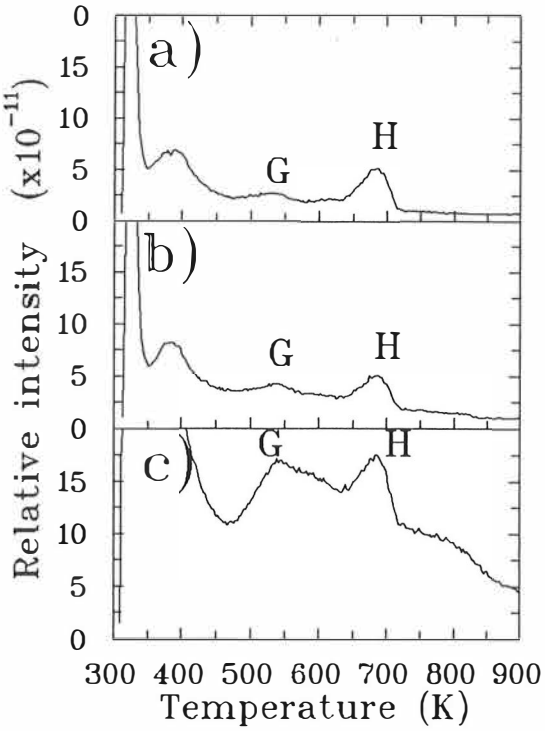

Figure 5.3. *Relative intensities of the G peak and the H peak. The spectra were measured after bombarding a copper single crystal with* 1.0 keV He^+ *ions with doses of a)* 10^{13}, *b)* $3 \cdot 10^{13}$ *and c)* 10^{14} *ions/cm*^{2}. *The G peak reflects a strong dose dependence.*

The most probable situation is that there are two helium atoms in a monovacancy, and one of them releases according to the scheme

$$He_2V \rightarrow He + HeV. \tag{5.4.}$$

To get a better justification for the interpretation of the G peak, another series of experiments was carried out as follows. First, the sample was implanted with 1.0 keV helium using a dose of 10^{13} ions/cm^2. Next a post-irradiation was performed using helium ion beam of 0.1 keV with different doses. As a third step, the sample was annealed at 400 K to eliminate surface-related traps. Finally, the sample was cooled down to room temperature, and a desorption spectrum was recorded.

The results of these experiments are presented in Fig. 5.4. and they indicate that the intensity of the G peak increases due to helium implantation with a low energy. The

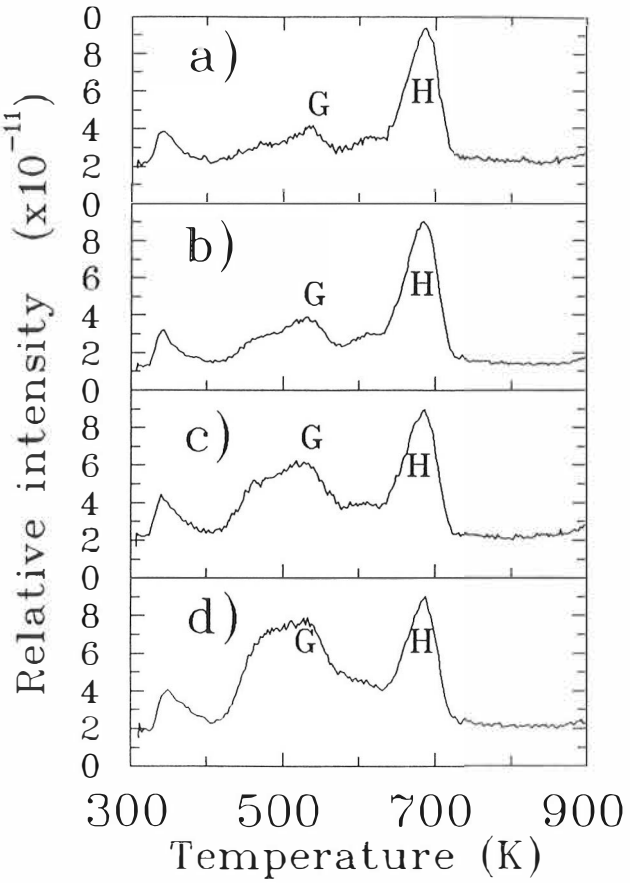

Figure 5.4. *Desorption spectra of copper implanted with* 10^{13} 1.0 keV He^+ *ions, post-implantated with* 0.1 keV He^+ *ions, annealed at 400 K for 10 minutes and finally heated from 300 K up to 900 K while monitoring the helium release. The doses of the post-irradiation are a) none, b)* $10^{13}/cm^2$, *c)* $3 \cdot 10^{13}/cm^2$ *and d)* $10^{14}/cm^2$.

observation supports our previous interpretation that the G peak has something to do with a defect filled with more than one helium. The width of the appearing peak indicates also that the G peak does not obey first-order kinetics or there are two defects so close to each other that they can not be separated. It is therefore possible that the activation energy associated with a monovacancy with two helium atoms inside is close to a monovacancy with a triple filling.

Buters et al. [68] have investigated the character of the X peak and to their opinion it can be associated with the reaction

$$He_2V_2 \rightarrow He + HeV_2. \qquad (5.5.)$$

Since the X peak appears when using bombarding energies of several keV, it is natural to assume that this peak can be related to helium release from a divacancy. According to Wilson et al. [**27**] the binding energy associated with the process expressed in Eq. (5.5.) is close to the binding energy of the helium release from a singly-filled monovacancy. Therefore it is natural that the X peak appears close to the H peak. The calculations do not exclude the possibility that the X peak could indicate helium release from singly filled divacancies.

The dose dependence of the X peak suggests, however, that it can not be associated with a defect with multiple filling, because the peak is visible when using relatively low doses. Another problem arises from the residual defect: one helium atom can not stabilize a divacancy, and it is probable that the defect-helium complex becomes mobile, diffuses step by step and disappeares at the surface. However, there is no clear indication of such a process in the desorption spectra.

To determine the nature of the X peak, a procedure similar to that of the investigation of the G peak was performed. Firstly, the sample was implanted with 3 keV He^+ ions. A fraction of the projectiles create divacancies. As a second step, the sample was post-irradiated with 0.1 keV He^+ ions to fill the singly-filled divacancies with another helium atom. Thirdly, the sample was annealed at 500 K for 10 minutes to eliminate the G peak. After cooling the sample to 300 K, a helium desorption experiment was carried out.

The results of the investigations of the X peak are shown in Fig. 5.5. The X peak becomes more clearly visible with increasing doses of 0.1 keV helium. This supports the assumption that the X peak indicates helium release from a He_2V_2 complex. As far as the puzzle of the remaining HeV_2 is concerned, it is possible that this defect becomes mobile and becomes annihilated at the surface. Since the temperature associated with such a process is close to the temperature corresponding to the appearance of the H peak, the helium release due to the annihilation of the HeV_2 complex can not be distinguished. Taking into consideration that the intensity of the X peak is essentially lower than the one of the H peak, the suggested mechanism might be a reasonable explanation for the X peak.

The fact that the intensity of the X peak does not depend very strongly on the implantation dose suggests that the corresponding defect is only singly filled with helium. Since

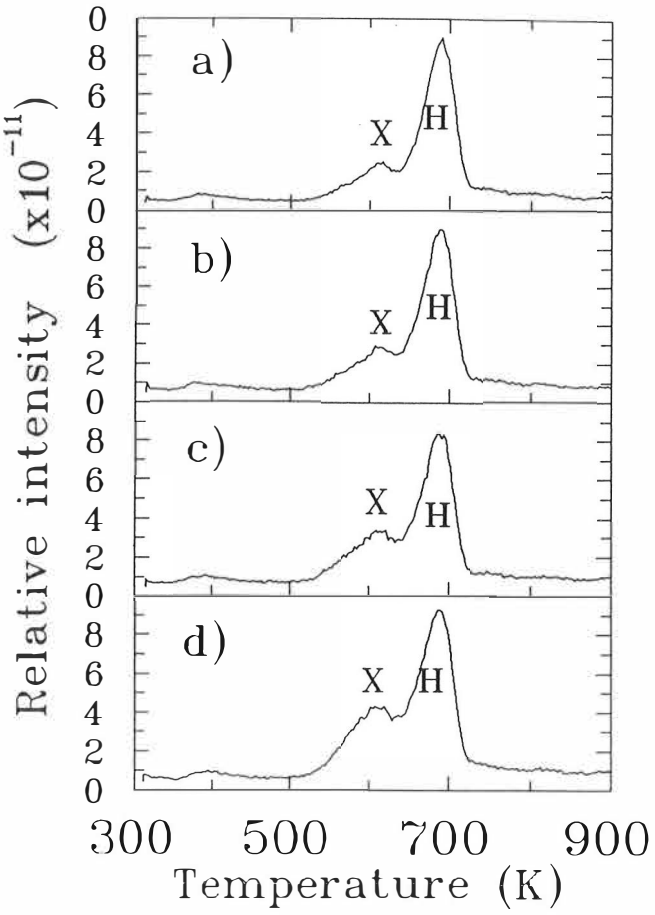

Figure 5.5. *Desorption spectra of copper implanted with* 10^{13} 3.0 keV He^+ *ions, post-implantated with* 0.1 keV He^+ *ions, annealed at 500 K for 10 minutes and followed by a helium desorption experiment. The doses of the post-irradiations are a) none, b)* $10^{13}/cm^2$, *c)* $3 \cdot 10^{13}/cm^2$ *and d)* $10^{14}/cm^2$.

this peak appears already when using doses of 10^{12} ions/cm^2, it is not likely that such a low dose may result in a multiple trapping of helium in a divacancy. It is not clear whether a HeV_2 complex can survive up to 600 K, because it can diffuse to the surface. According to theoretical predictions the dissociation energy of such a complex does not differ essentially from the dissociation energy of a helium-filled monovacancy [**27**]. All in all, the dose dependence of the X peak might be a more reliable evidence concerning the nature of the X peak than the decoration of defects with low-energy helium atoms. To summarize, the results indicate that the X peak can be associated most probably with a

singly-filled double vacancy.

The intensity of the I peak increases remarkably with increasing bombarding energy and dose. This implies that the I peak describes helium release from larger defect complexes. A relatively strong dose dependence indicates also that these defects are multiply filled with helium. Unfortunately the maximum measuring temperature had to be limited to 900 K, and hence a clear indication of the stability of the I peak at high temperatures could not be obtained. (The temperature tends to oscillate after exceeding 900 K.) However, the I peak did not appear in the measuring range after annealing the sample at 1000 K.

Since the I peak is relatively stable at high temperatures, it is likely that it is related to defect complexes in which a multiple vacancy is filled with several helium atoms, which stabilize the defect and hinder the diffusive motion. A summary of the peaks appearing in helium desorption spectra of copper is presented in Table 5.1.

Table 5.1. *Interpretation of the different helium peaks in copper.*

Peak	Suggested mechanism	Argument
G	$He_2V \rightarrow He + HeV$	Strong dose dependence
X	$HeV_2 \rightarrow He + V_2$	Low doses, high energies
H	$HeV \rightarrow He + V$	Threshold energy, weak dose dependence
I	$He_mV_n \rightarrow He + He_{m-1}V_n$	Appears with high energies and doses

The peak appearing at the very beginning in the spectra is most likely due to helium release from the boron nitride oven used for heating the sample. This was confirmed by bombarding the rear face of the oven with helium beams, when the sample itself is totally hidden. During the heating cycle, a sharp peak at around 330 K was observed. Moreover, if the temperature exceeded 400 K, the signal of the mass spectrometer attained the background level. Therefore, the effects due to boron nitride do not interfere with the peaks discussed in this chapter.

Another peculiar phenomenon is the peak appearing at around 400 K. There is some evidence that this peak has something to do with the purity of the surface, because it is nearly invisible just after cleaning the sample with sputtering/annealing cycles. On the other hand, the effect becomes less visible, if the bombarding energy increases. The same peak was observed in the measurements performed by Buters et al. [68]. This effect is

an indication of surface-related traps or imperfections within the first few atomic layers. The same difficulties have been met when investigating nickel [**72,73**]. The shape of the peak in question might refer to diffusive release of helium, but it is hard to explain the actual mechanism of such a process.

5.3. Activation energies for helium peaks

The shape of the H peak is in accordance with the theory of first-order kinetics. Within the accuracy of the temperature measurement, the H peak seems to appear at the same temperature independent of the dose or the bombarding energy. Since this peak is also clearly visible, the activation energy of the corresponding release process was estimated using different methods.

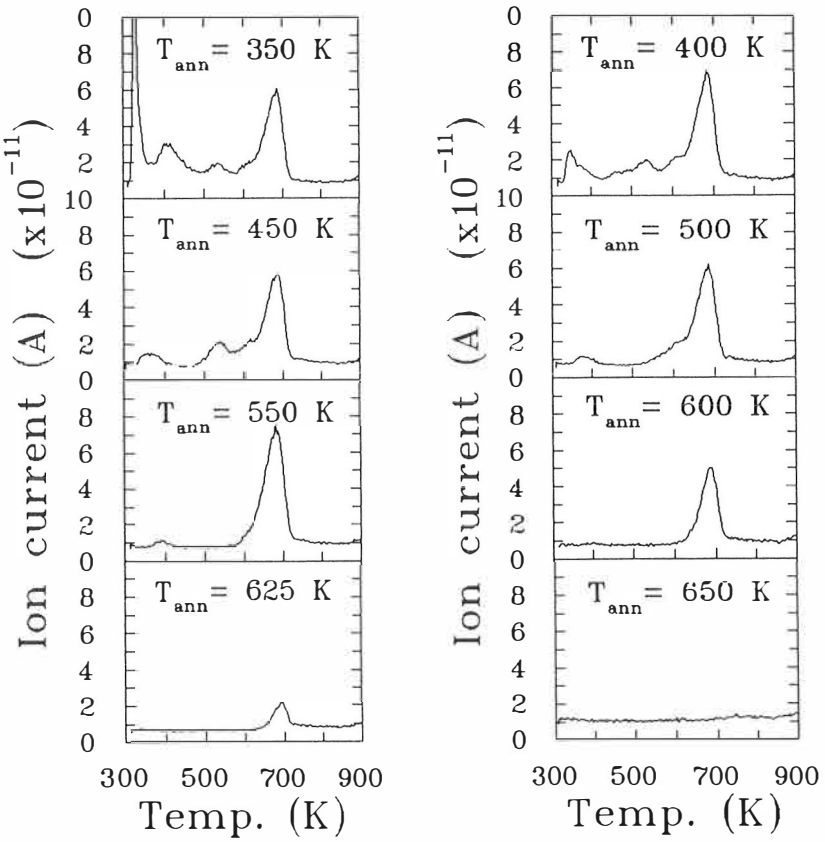

Figure 5.6. *Stability of the H peak measured after different annealing temperatures. For more information see the text.*

The stability of the H peak against ramp annealing cycles is shown in Fig. 5.6. The sample was bombarded with 1.0 keV He^+ ions with a dose of 10^{13} ions/cm^2. Next the sample was annealed at a certain temperature for 10 minutes. Finally, the sample was cooled down to 300 K and a desorption spectrum was measured. The spectra presented in Fig. 5.6. were measured using a heating rate of 1.0 K/s.

When using low annealing temperatures, only the beginning of the spectrum disappears step by step but the H peak remains unchanged. The H peak does not start to decrease in intensity until at around 600 K. On the other hand, since the intensities of the H peaks are equal, one can conclude that the reproducibility of the experiments is very good. After annealing at 600 K, the population of the H peak was reduced about 25 %. The peak totally disappears after annealing at 650 K.

Although the population of the H peak is slightly reduced after annealing at 600 K, such a procedure makes it possible to create a spectrum containing just the H peak because the intensities of the G and X peaks are essentially zero and the clustering, usually observed at higher temperatures, is not visible with a bombarding energy of 1.0 keV. Therefore, a peak-fitting procedure, described in chapter 3.4., was applied to a spectrum obtained after annealing the sample at 600 K.

The measured spectrum and the corresponding theoretical fit is shown in Fig. 5.7. The activation energy was found to be very close to 2.0 eV with the rate constant of $2.0 \cdot 10^{13}$ 1/s. The fit is not very sensitive to the determination of the background level; usually the global minimum of the measured ion current represents a reasonable background level. The error of E_D was found to be 0.10 eV which means that the error of the rate constant is very large ($\nu_o = 10^{13.3 \pm 0.8}$ 1/s).

It should be noted that the parameters derived from the peak-fitting procedure are in agreement with the annealing experiments presented in Fig. 5.6. For example, it can be predicted that after annealing at 600 K, the intensity of the H peak has decreased about 20 % (see the definition of the relaxation time in chapter 2.3.). Furthermore, at T = 650 K the corresponding relaxation time is essentially shorter, and the initial number of helium atoms is reduced by a factor of 100, which implies that the H peak practically disappears.

The peak-area method, when applied to this particular case, gives E_D=(2.10±0.10) eV. The error limits were estimated by analysing the same spectrum several times choosing

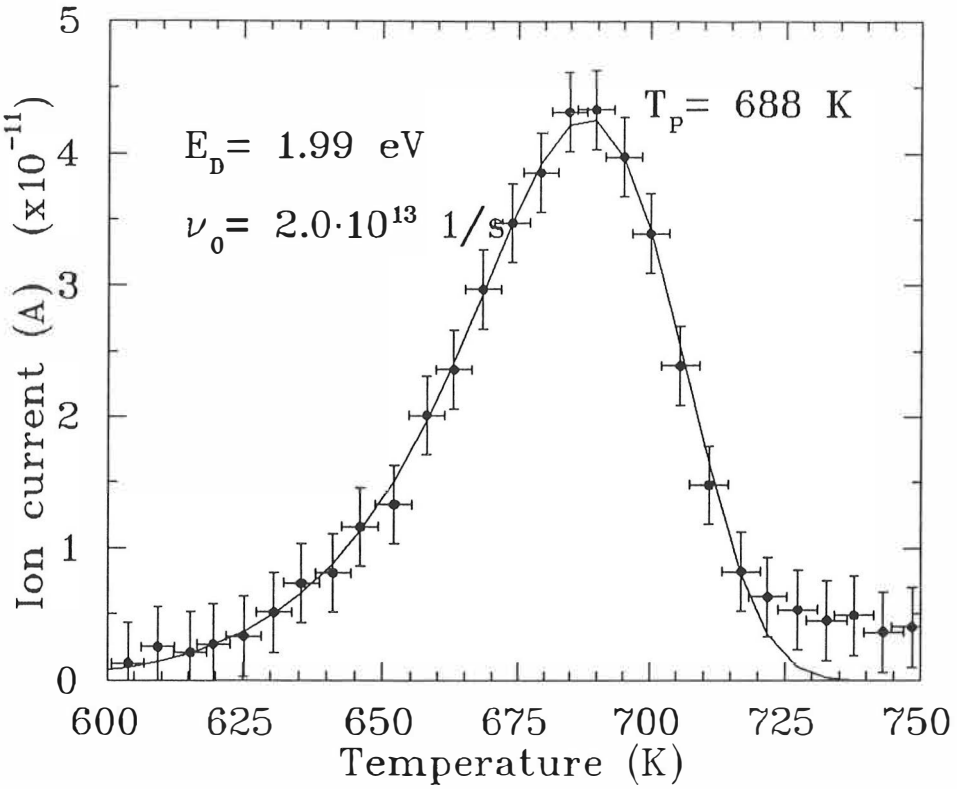

Figure 5.7. *Determination of the kinetic parameters of the H peak. The experimental data points are marked with solid circles and error bars and the solid line represents a least-squares fit with the indicated parameters.*

different values for T_1 and T_2. The rate constant was found to be $\nu_o = 10^{14.1\pm0.8}$ 1/s. Some difficulties were met in the determination of the net integral of the spectrum corresponding to the actual number of desorbing particles.

To determine the activation energy by using the Arrhenius method, several spectra were measured with different heating rates. In each case, the sample was annealed at 600 K before measuring the helium release. The spectra are shown in Fig. 5.8. The peak temperature has a clear tendency to increase with increasing heating rate.

The corresponding Arrhenius plot is shown in Fig. 5.9. The activation energy extracted from a least-squares fit was (2.19±0.08) eV and the rate constant was found to be $\nu_o = 10^{14.7\pm0.7}$ 1/s. Also in this case, the error in the determination of the rate constant is unreasonably large because the rate constant depends exponentially on E_D.

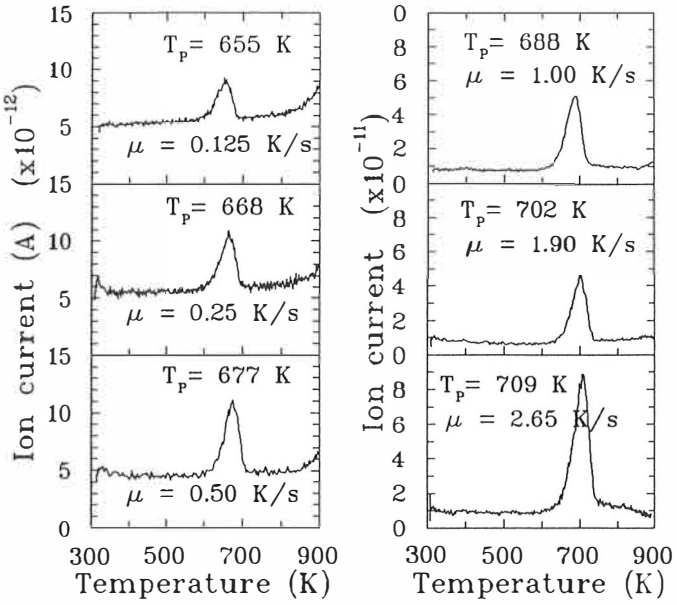

Figure 5.8. *Helium desorption spectra after bombarding a copper single crystal with* 1.0 keV He^+ *ions, annealing at 600 K and subsequently heating the crystal from 300 K up to 900 K with different heating rates.*

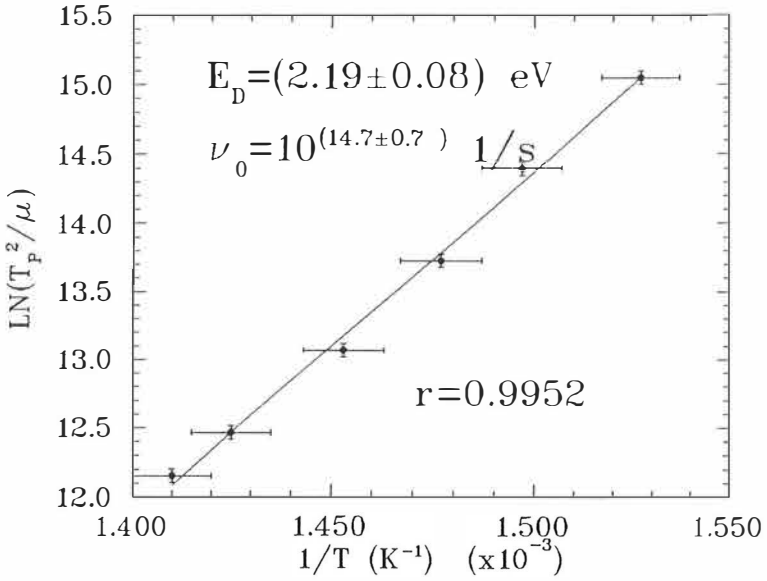

Figure 5.9. *Arrhenius plot for determining the activation energy of the H peak. The plot is related to the spectra illustrated in Fig 5.8.*

The activation energies associated with the G peak and the X peak were estimated by means of the corresponding peak temperatures and arbitrary rate constants. The G peak was observed at $T_{P,G} = 540 \pm 2$ K, and the X peak at $T_{P,X} = 610 \pm 2$ K. Assuming that the rate constant is $\nu_o = 10^{13.0\pm1.0}$ 1/s (which evidently is a rather good approximation), the corresponding activation energies for the G peak and for the X peak are 1.52±0.11 eV and 1.73±0.13 eV, respectively.

5.4. ^{3}He experiments

The rate constant is usually expected to be independent of temperature. On the other hand, the vibrations of a trapped atom in a lattice may be due to lattice phonons. Another, a purely classical model assumes that a helium atom, trapped in a vacancy, can be treated as a harmonic oscillator, and the vibration frequency is determined by the mass of the atom, as well as by the curvature of the potential well. The latter model predicts that the vibration frequency depends on the mass of the impurity.

Since the helium-metal interaction is determined by the local electron density, it depends mainly on the host metal lattice and on the electron configuration of the impurity. There is hardly any difference in electronic structure between ^{3}He and ^{4}He. Therefore, if ^{4}He is replaced by ^{3}He in thermal desorption experiments, the effective potential felt by a helium atom remains unchanged, and the only effect that might be observed is due to the change in mass.

If the model based on a harmonic oscillator is accepted, the vibration frequency can be written as

$$\nu_o = \sqrt{\frac{\left(\frac{d^2U}{dx^2}\right)}{4\pi^2 m}}. \qquad (5.6.)$$

Thus, a classical treatment of the problem predicts that the rate constant is inversely proportional to the square root of the mass of the desorbing atom. Consequently, when ^{4}He is replaced by ^{3}He, the rate constant of a desorption process will increase by a factor of $(4/3)^{1/2} \approx 1.15$.

Some results of experiments using ^{3}He beams are shown in Fig. 5.10. For comparison, the results of experiments carried out with ^{4}He are drawn in the same windows. No

remarkable differences concerning the dependence on bombarding energy or dose can be observed.

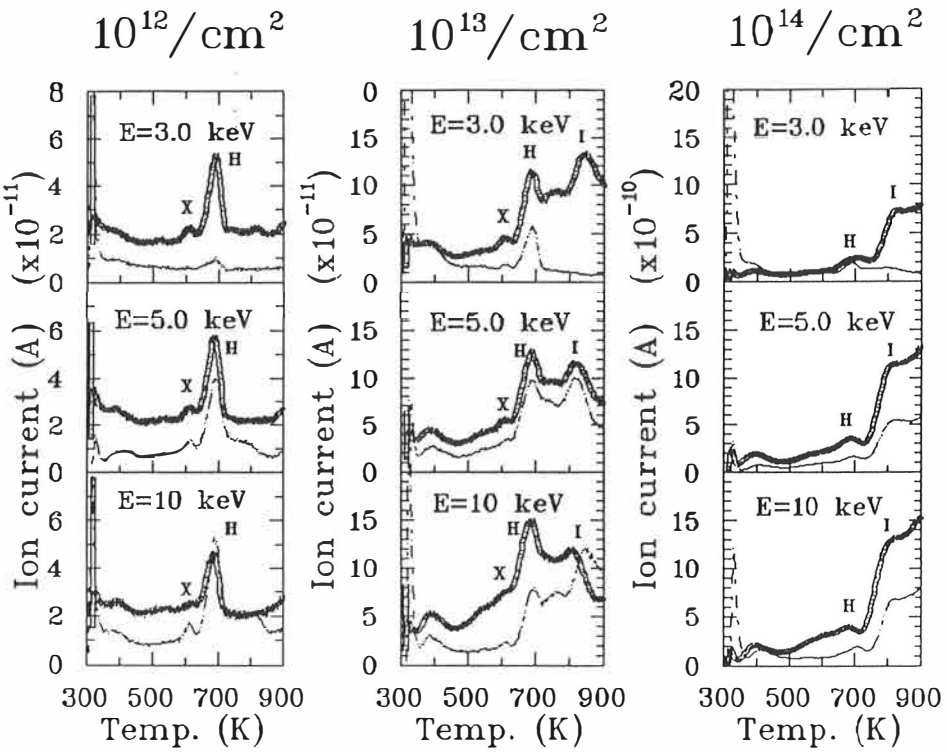

Figure 5.10. *Desorption spectra of* ^{3}He *in copper with different doses and bombarding energies (thicker line) compared to the corresponding experiments using* ^{4}He *(dashed line).*

In fact, the spectra obtained from the ^{3}He experiments differ from the ones of the ^{4}He experiments in two ways. Firstly, the background level seems to be a little bit higher. This is evidently due to the ^{3}He load from the ECR ion source via the differential pumping section. Although the connection to the ECR beam line is designed in such a way that the gas load from the beam line is negligible, the throughput of the differential pumping section for ^{3}He is relatively high, mainly because of the high thermal speed of ^{3}He. For the same reason, the turbo pump of the desorption facility can not remove the ^{3}He atoms very effectively.

The second characteristic difference is that the intensities of the ^{3}He spectra tend to be higher than the ones of the ^{4}He spectra. This is not expected to reflect any profound

physical effect. The intensities observed in Fig. 5.10. correspond to the initial ion currents recorded by the mass spectrometer and no calibration procedure was performed. Moreover, the current density of the ECR ion beam may alter during the experiments and the local particle flux may be different, although the total doses are equal.

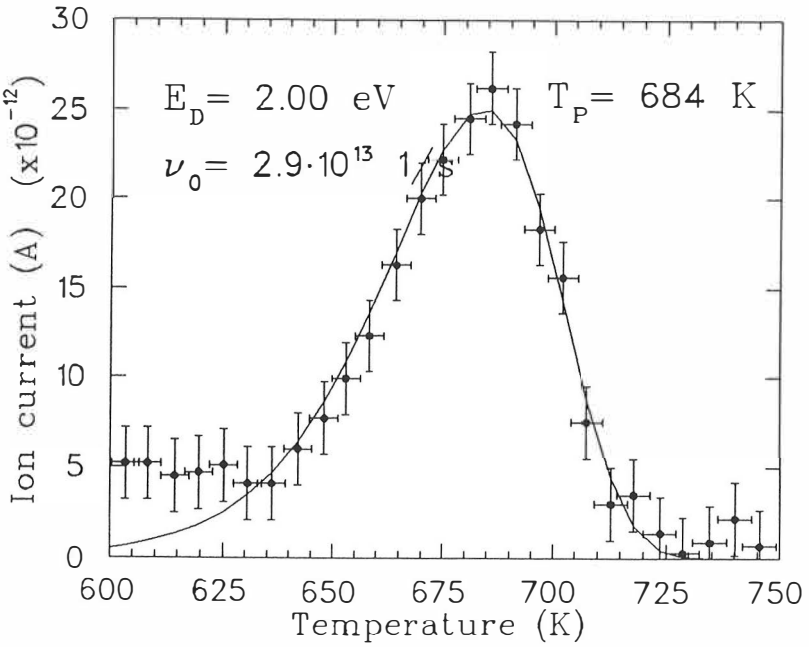

Figure 5.11. *Determination of the kinetic parameters of the H peak in* ^{3}He *experiments. The parameters of the first-order kinetic model do not differ essentially from the case of* ^{4}He.

Within the accuracy of the temperature measurement, only a slight peak shift due to the isotope effect can be observed. One example of the H peak of ^{3}He experiments is shown in Fig. 5.11. The kinetic parameters extracted from a peak-fitting procedure are very close to the values obtained in the case of ^{4}He.

Actually, if the isotope effect boils down to Eq. (5.6.), the value of the rate constant increases by a factor of 1.15 when ^{4}He is replaced by ^{3}He. Using the parameters obtained in chapter 5.3. one can predict that the rate constant of the H peak attains a value of $2.3 \cdot 10^{13}$ with the activation energy of 2.0 eV. This means that the temperature of the H peak decreases about 2 K.

The peak-fitting procedure in Fig. 5.11. indicates that the H peak appears at a lower temperature in the case of ^{3}He. Anyhow, the accuracy of this method is limited because

of relatively large statistical errors, and hence the isotope effect can not be demonstrated properly. We may conclude that the isotope effect has only a tiny influence on a helium desorption spectrum, as predicted by the first-order rate equation.

5.5. Low-temperature measurements

A copper single crystal was bombarded with 10^{13} He^+ ions at 200 K using different energies. The sample was heated from 200 K up to 900 K with a heating rate of 1.0 K/s. The ion currents vs temperature are shown in Fig. 5.12.

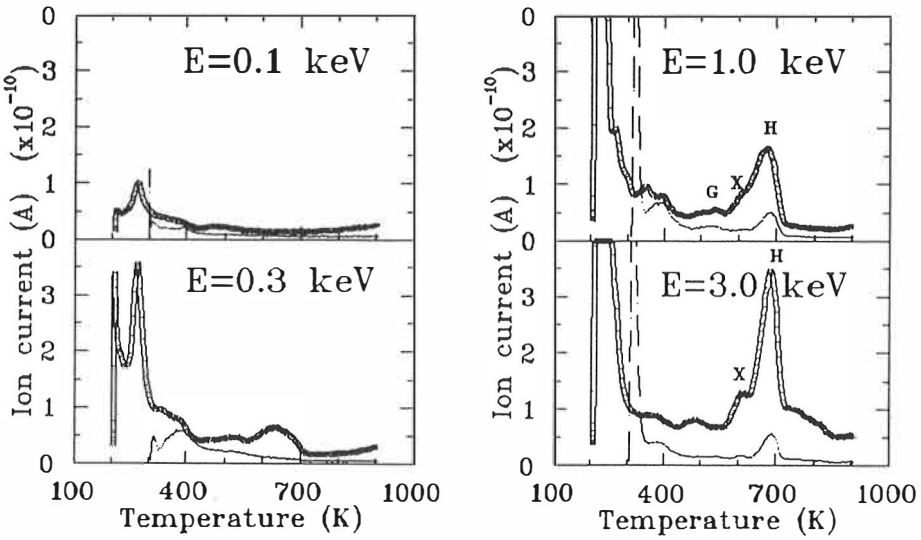

Figure 5.12. *Helium desorption spectra after irradiating at 200 K (thicker line) compared to the experiments carried out at room temperature (dashed line).*

The most visible difference between these spectra and the ones corresponding to irradiation at room temperature is associated with the increasing populations of the peaks X and H, which indicate helium release from singly filled divacancies and monovacancies, respectively. For example, when the sample was irradiated with 3.0 keV He^+ ions at 200 K, the sum of the population of the X peak and the H peak increased by a factor of 6.7 when compared to the case when the sample was irradiated at room temperature. When the bombarding energy was 1.0 keV, the intensity was more than three times larger than for the experiment carried out at room temperature.

Although the spectra are not converted to absolute desorption rates, the sensitivity of the mass spectrometer was checked during the experiments. The differences in the peak intensities can not be explained by different experimental conditions or by errors in dose determination. Therefore, the effect observed is due to the different irradiation temperature. At room temperature, when both copper vacancies [**61**] and interstitial helium are mobile, a major fraction of the vacancies escape without being decorated with helium. At 200 K vacancies become immobile, and the probability of filling them with helium is essentially higher.

As discussed in chapter 2.3., the migration energy of interstitial helium in copper has been calculated to be about 0.6 eV. Furthermore, when bombarding copper with 3.0 keV He^+ ions, the penetration of ions is 100±50 atomic layers according to the TRIM calculations [**74**], and the implantation profile can be approximated as a gaussian distribution. If such an implantation is performed at 200 K, the diffusion model described in chapter 2.3. predicts that the maximum of the corresponding diffusion peak would be observed at 295 K, provided that a heating rate of 1.0 K/s is used. Since such a diffusive release was not observed, it supports the assumption, presented by many theoreticians [**29**], that the calculated migration energies may be overestimated, because, for instance, the relaxation effects in the lattice are always relatively difficult to take into account.

Some attempts were made to find out whether the migration energy of helium in copper can be determined by measuring the corresponding diffusion distribution. A clear result was not obtained. This was caused by the fact that temperatures well below 200 K were beyond the performance of the cooling system. Moreover, the possibility that such a helium release is due to imperfect surface can not be excluded. A fraction of the ions can also encounter the oven made of boron nitride, and hence the signal observed at the very beginning of the heating cycle does not necessarily indicate interstitial migration.

The most tangible indication of interstitial diffusion was obtained by bombarding a copper single crystal with 3.0 keV He^+ ions at 150 K, followed by a heating cycle up to 300 K. A distribution similar to simulated diffusion spectra was observed at T = 180 K. The diffusion peak is shown in Fig. 5.13. However, the behaviour of the peak with different heating rates was not consistent with the prediction of the diffusion model. Therefore, no profound conclusions can be drawn concerning the migration energy of He in copper.

It is possible that the observation represents an upper limit for the migration energy of

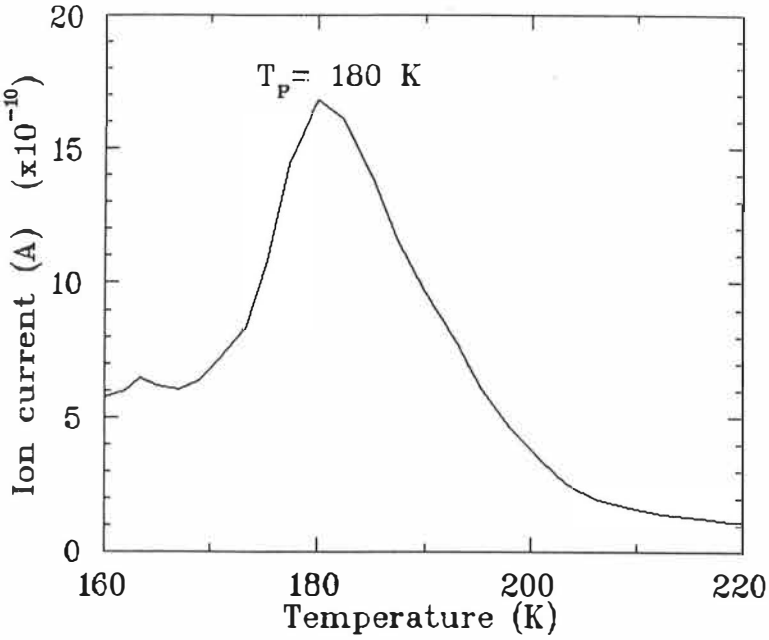

Figure 5.13. *Helium release vs temperature in the case of suspected interstitial migration. For further information see the text.*

helium in copper. A straightforward interpretation, using the diffusion model, predicts that the value of the migration energy is 0.36±0.02 eV, assuming that the helium release is controlled by interstitial diffusion. One has to bear in mind that the implantation itself introduces vacancies and self-interstitials in the target, and these defects, as well as multiply-filled interstitial sites, might bear some contribution when explaining the migration of helium at low temperatures [**23,40**].

6. Argon and neon in copper

When using heavier noble gases than helium in implantations, two clear differences concerning the basic physics can be stated. Firstly, due to their mass, heavy noble gas ions can transfer energy to target atoms more effectively. It follows that the penetration depth of heavy noble gas ions is essentially smaller than in the case of helium and the production of point defects is very effective. Secondly, when the size of the impurity increases, its mobility may decrease.

This chapter reviews some thermal desorption experiments in which a copper single crystal was bombarded with argon and neon and the corresponding gas release was measured with a mass spectrometer.

6.1. Argon in copper

A copper single crystal was bombarded with Ar ions at 200 K with a subsequent heating from 200 K up to 900 K using the standard heating rate of 1.0 K/s while monitoring the argon release with a mass spectrometer. The spectra are shown in Fig. 6.1.

The peaks appearing in Fig. 6.1. are essentially wider than the ones of helium. Another striking feature is the double peak that appears when using relatively low bombarding energies ($E \leq 5.0$ keV) and doses. These peaks are too wide to be dealt with the first-order model, but they might also be influenced by some effects that can not be resolved.

In the case of argon-implanted nickel, Edwards has observed similar peaks, interpreted as corresponding to argon release from substitutional traps [**75**]. According to Edwards, the peak at the lower-temperature side would be due to argon trapping within the first atomic layers, while the other peak, appearing at higher temperature, would correspond to substitutional traps located deeper in the crystal.

The peak temperatures, observed by Edwards, were 542 K and 656 K when using heating rates of 16.6 K/s and 18.4 K/s, respectively [**76**]. In the present case of copper, when the heating rate was about one order of magnitude lower, the argon peaks appeared at

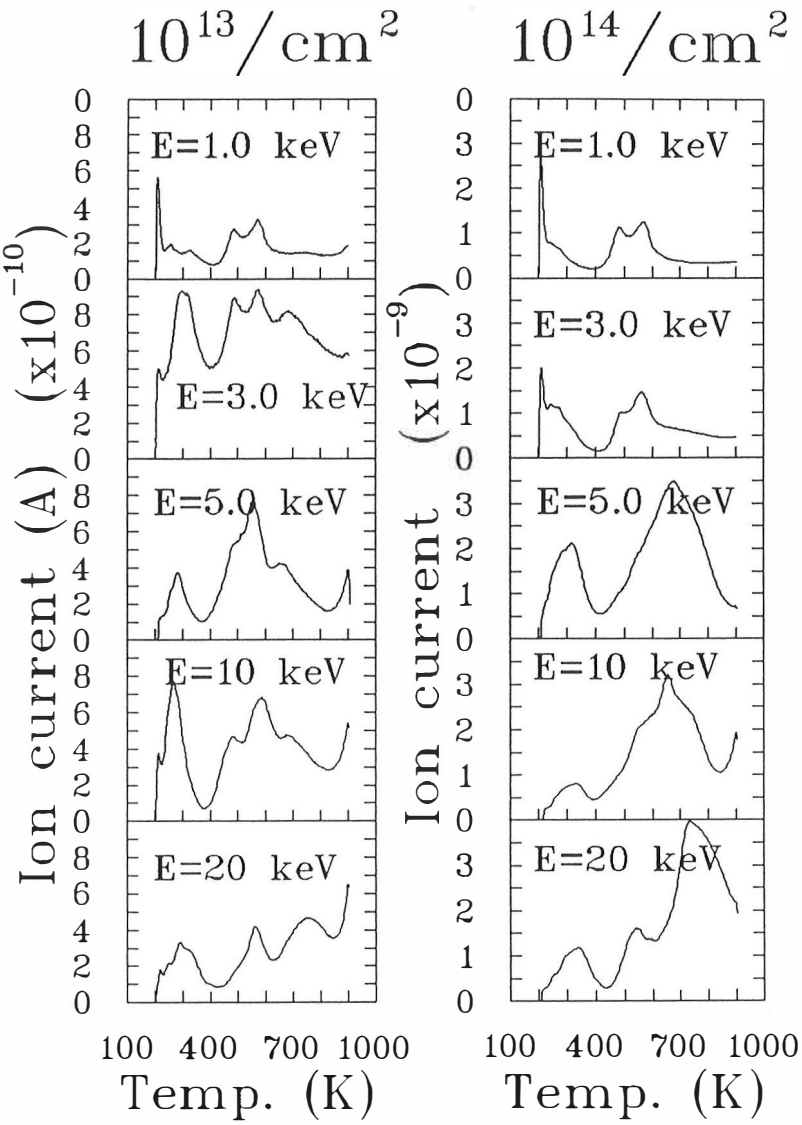

Figure 6.1. *Argon desorption spectra with different bombarding energies and doses.*

around 485 K and 570 K. Taking into account the difference in heating rates, one can deduce that the behaviour of argon is very similar both in nickel and in copper. This is a natural conclusion, because both of them are FCC metals with nearly equal atomic masses.

The scheme that heavy noble gases, escaping from different depths, can be observed as separated peaks has also been proposed by Kornelsen and Sinha [77] in the case of

noble-gas-implanted tungsten. Their interpretation was based on the fact that certain desorption peaks depended strongly on the orientation of the target crystal. In the case of copper, this interpretation was tested by bombarding the sample using different angles of incidence, but no changes concerning the intensities of these peaks were observed. In any case, these experiments are not conclusive enough to rule out or confirm this theory of desorption from different depths.

The double peak appearing in Ar spectra might be due to argon release from monovacancies and divacancies. Since the peak observed in the higher-temperature region grows up in intensity with increasing bombarding energies, it might represent the double vacancy case. However, such an interpretation would lead to the scheme where the dissociation energy for a complex consisting of a vacancy filled with argon is essentially lower than the activation energy related to the H peak in the case of helium. There might be some physical facts that would support this behaviour [**78**], but it can not be verified without careful calculations with realistic metal - noble gas interactions.

The distribution appearing in the high-temperature region in argon spectra can be considered as a vacancy cluster with a variable filling with argon. As in the case of helium, the peak appears with high bombarding energies and depends strongly on the bombarding dose. The maximum of the peak depends slightly on the bombarding energy, and if the experiment is repeated under the same conditions, the maximum of the peak may vary randomly about ± 10 K. The same peak has been observed previously in the case of Xe-implanted copper [**79,80**], and it is assumed to be due to diffusive release of argon starting its random walk several atomic layers below the surface. Presumably the argon release is assisted by thermal vacancies.

The microscopic phenomena related to argon release from copper are evidently more complicated than the ones related to helium. It is not likely that argon release can be described by a single-jump mechanism combined with a rapid migration to the surface. The dose dependence of the spectra shown in Fig. 6.1. suggests that the double peak can be associated with singly-filled traps, whereas the high-temperature peak is due to multiply-filled defect clusters. The interpretation that argon atoms, starting their random walk at different depths, can be observed as different peaks is not very realistic, and it is also against the predictions of the diffusion model described in chapter 2.3.

It is obvious that due to the size of argon atoms, the lattice is strongly relaxed. This leads

to strong deformation of argon-filled vacancies and interstitial sites. Moreover, de Hosson [81] has stated that, according to atomistic calculations, the strain energy of an interstitial argon atom in copper is so high that a self-trapping effect is possible, i.e. an argon atom can occupy a substitutional site by pushing a copper atom to interstitial position. If such a process is possible, it may account for the complexity of argon desorption spectra. Such complexity has been observed also in the case of argon-implanted molybdenum [**82,83**].

6.2. Neon in copper

Some desorption spectra were recorded after bombarding a copper single crystal with neon beams. The spectra are shown in Fig. 6.2. The experimental details are similar to those of the argon experiments.

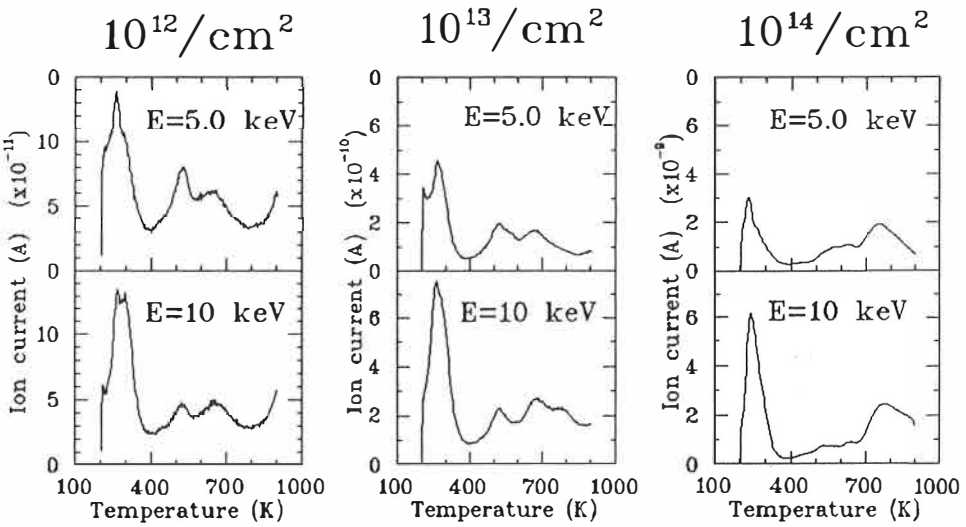

Figure 6.2. *Neon desorption spectra of copper.*

The behaviour of neon in copper does not differ essentially from that of argon. There are, however, some differences.

At the beginning of the heating cycle, a strong neon release is observed, which may be due to escaping neon interstitials. The maximum of the peak is observed at 250±20 K, depending slightly on the bombarding dose and energy. If this peak indicates a pure interstitial diffusion, the model described in chapter 2.3. predicts that the migration

energy for Ne in copper would be $E_M = 0.50 \pm 0.05$ eV. Anyhow, it is probable that there are also other mechanisms to explain the neon release.

The double peak observed in argon desorption spectra is present also in the case of neon. The peak temperatures are 520 K and 660 K, when the spectra are recorded with a heating rate of 1.0 K/s. As in the case of argon desorption spectra, the latter maximum of the double peak becomes more visible with increasing bombarding energies. The intensity of the double peak depends only slightly on the irradiation dose. Evidently, the peaks are related to similar traps as in the case of neon-implanted nickel [**75,76**].

In the high-temperature region, a broad gas-release distribution was observed. Since the peak appears when using high doses, it can be associated with clusters containing several neon atoms. It is also possible that the mobility of this complex is assisted by thermal vacancies.

When the bombardment is performed with neon instead of argon, the double peak seems to shift about 50 K towards higher temperatures, a trend observed also by Edwards [**76**]. It is thus possible that in the case of both argon and neon, the double peak indicates noble gas release from similar defects. In addition, the binding energy for neon in the traps seems to be slightly higher than that of argon. Since the traps filled with neon are more stable, it is not likely that we are dealing with simple point defects. For instance, if the double peak indicates neon release from singly-filled monovacancies (T = 520 K) and divacancies (T = 660 K), it means that a divacancy filled with argon becomes more stable if argon is replaced by neon. It is clear that such a behaviour is not very realistic.

A more consistent interpretation is obtained, if the latter one of the two peaks represents noble gas release from monovacancies and the former from singly-filled double vacancies. Such a theory predicts that the heavier the noble gas atom is, the weaker it is trapped by a simple point defect. It might be possible, that a relatively big noble gas atom, such as argon, is not as sensitive to the change in electron density in a vacancy as helium. The binding energies of argon and neon in a copper vacancy will be calculated in the near future using a multicomponent version of the effective-medium theory [**84**].

Especially in the case of neon, the jumps in the double peak can not be explained by desorption from different atomic layers. For example, in the case of the 10 keV neon, the average penetration depth is about 50 atomic layers with the angle of incidence being 30 degrees. It is hard to believe that in such a case the first few atomic layers would give

a remarkable contribution to the desorption spectra. Moreover, if the first peak in the neon spectra is due to interstitial migration, the corresponding migration energy is 0.50 eV. Hence, at T = 520 K, where one of the neon peaks exists, the mean diffusion time through 50 atomic layers is of the order of 10 μs, estimated by using a simple harmonic diffusion model (see chapter 2.3.). Therefore it is impossible that the double peak would be due to delay caused by the limited mobility of neon.

Altogether, the behaviour of neon and argon in copper is rather complicated and there are still many unsolved questions. Obviously, there are many contributing things such as strong lattice relaxation, clustering of vacancies, capture of interstitials [**83**] etc. that account for the big difference between the behaviour of helium and the heavier noble gas atoms.

7. He-Ne and He-Ar interactions in copper

The fact that helium is strongly trapped by point defects makes it possible to use interstitial helium as a tool to probe vacancies and vacancy clusters. The defects can be created in a controlled manner by irradiation with heavy noble gas ions. After performing a desorption cycle the sample can be annealed and hence the same sample can be used for further experiments.

Helium-probing experiments have been previously reported on tungsten and molybdenum [**83,85,86**]. These materials are rather well investigated and the behaviour of vacancies as well vacancy-impurity interactions are relatively well understood. In the case of nickel the data is not as consistent [**87**], presumably because of the FCC structure of nickel. Since the packing density of the FCC metals is usually higher than the one of the BCC metals, such as tungsten, the penetration of helium ions, injected with a subthreshold energy, might be more difficult. Some further difficulties may arise from the mobility of vacancies in the FCC metals. In particular, the copper vacancies become mobile at 220 K [**61**], which means that the irradiations related to helium-probing experiments have to be made at 200 K or below.

Since the behaviour of helium in copper was thoroughly investigated in chapter 5, helium-filled vacancies can be easily identified if such complexes can be formed when probing a deformed crystal with helium ions. In this chapter some attention is paid to the question whether the helium-probing technique can be applied to investigations of point defects in copper.

7.1. Room temperature measurements

To study if some impurities implanted in copper crystal have any influence on the trapping of helium, some helium desorption spectra were measured after irradiating the target with argon ions. The irradiations were carried out at room temperature, which means that pure copper vacancies are not stable at that temperature. The spectra were found to be strongly distorted due to argon preimplantation.

A typical effect due to argon impurities is shown in Fig 7.1. As mentioned in chapter 5.1., He^+ ions implanted with an energy of 3.0 keV can create vacancies, and there is clear evidence in the corresponding desorption spectrum of helium-filled vacancies (the H peak). If the sample is prebombarded with 3.0 keV Ar^+ ions, the spectra become strongly modified. Especially, when the dose of argon bombardment is as high as $10^{14}/cm^2$, the H peak is hardly distinguished from other effects appearing within the temperature range of 500 K - 700 K.

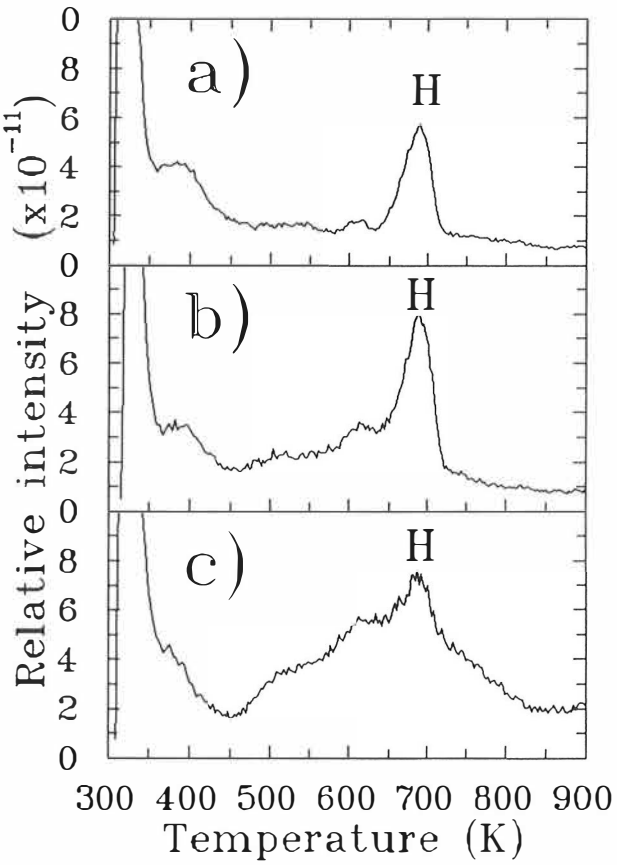

Figure 7.1. *Modification of helium desorption spectra due to preimplantation by* 3.0 keV Ar^+ *ions. The helium implantations were performed with* 3.0 keV He^+ *ions with a dose of* 10^{13} ions/cm^2. *The doses used in argon prebombardment are a) none, b)* $10^{13}/cm^2$, *and c)* $10^{14}/cm^2$.

It should be noted that the intensity of the H peak does not decrease; the distortion can be explained by assuming that the argon implants as such are favourable traps for helium. It

is also possible that vacancies, that in the case of copper are mobile at room temperature, are trapped by Ar impurities. As a result, helium is trapped by argon-vacancy clusters. Since argon in copper can be regarded as an oversized impurity, this mechanism is very probable. Similar behaviour has been observed previously in the case of indium-implanted copper [88].

If the argon irradiation is performed after helium implantation, a fully different behaviour can be observed. This effect is shown in Fig. 7.2., when a copper single crystal is bombarded with 1.0 keV He^+ ions with a dose of $10^{13}/cm^2$ followed by a post-irradiation with 3.0 keV Ar^+ ions using different doses.

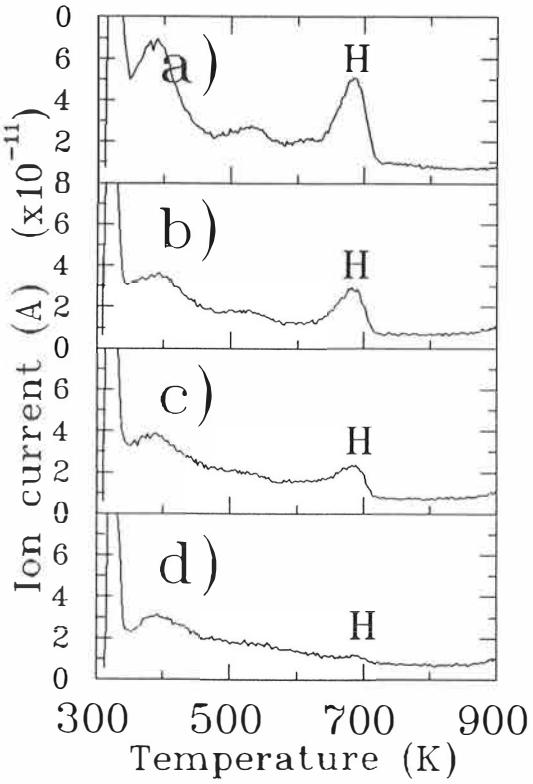

Figure 7.2. *Helium desorption spectra of copper, bombarded with* 10^{13} 1.0 keV He^+ *ions and subsequently irradiated with* 3.0 keV Ar^+ *ions. The argon doses are a) none, b)* $10^{12}/cm^2$, *c)* $10^{13}/cm^2$, *and d)* $10^{14}/cm^2$. *For further information see the text.*

It was found that relatively small doses of the argon bombardment ($10^{12}/cm^2$) reduce the intensity of the H peak. If the argon dose is $10^{14}/cm^2$, the H peak nearly disappears.

Since the energy received by the target during such a bombardment is 48 μJ, the global heating of the sample can be excluded, and the influence of argon post-bombardment is a purely microscopic effect.

It is well known that an ion bombardment carried out with heavy noble gas ions is an effective method to create mobile self-interstitials that can recombine with point defects within the first tens of atomic layers [**83**]. In this particular case this means that the self-interstitials, created by argon bombardment, are annihilated with helium-filled vacancies

$$HeV + SI \rightarrow He_{\mathrm{IS}}. \qquad (7.1.)$$

As a result, a substitutional helium atom is pushed to interstitial position. Since interstitial helium in copper is mobile at room temperature, most of the He atoms, kicked out by self-interstitials, escape at the surface before they can be detected. It is also seen in Fig. 7.2. that the contribution, usually present in helium desorption spectra at around 400 K, reduces after performing the post-bombardment, which implies that this effect can be associated with imperfections close to the surface.

According to the TRIM calculations, the maximum range of 1.0 keV He^+ and 3.0 keV Ar^+ ions are 80±40 Å and 25±15 Å, respectively. Since the experiments were made at room temperature, there are no stable vacancies present, and the trapping of helium atoms occurs at the end of the collision cascade. Thus, it is possible that there is a mechanism to extend the range of self-interstitial collisions deeper in the crystal. Such a mechanism might be based on row collisions generated by dumb-bell configurations, which are frequently suggested for describing the mobility of self interstitials in FCC metals [**89**]. On the other hand, the results of the TRIM calculations must not to be taken too seriously, because the program assumes the target to be amorphous material without a well-defined lattice structure.

7.2. Helium-probing experiments

Point defects produced by heavy noble gas ions were studied by bombarding a copper single crystal with keV-range Ar ions followed by He injection (0.3 keV, $10^{13}/\mathrm{cm}^2$). The irradiations were performed at 200 K, which according to present knowledge is below the

stage III in copper [13,61, 90-92]. The helium bombarding energy was intentionally chosen above the displacement threshold energy in copper to enhance the penetration of helium ions which was expected to be a limiting factor in the experiments. The experiments were carried out using various energies and doses for argon. A summary of the experiments is shown in Fig. 7.3.

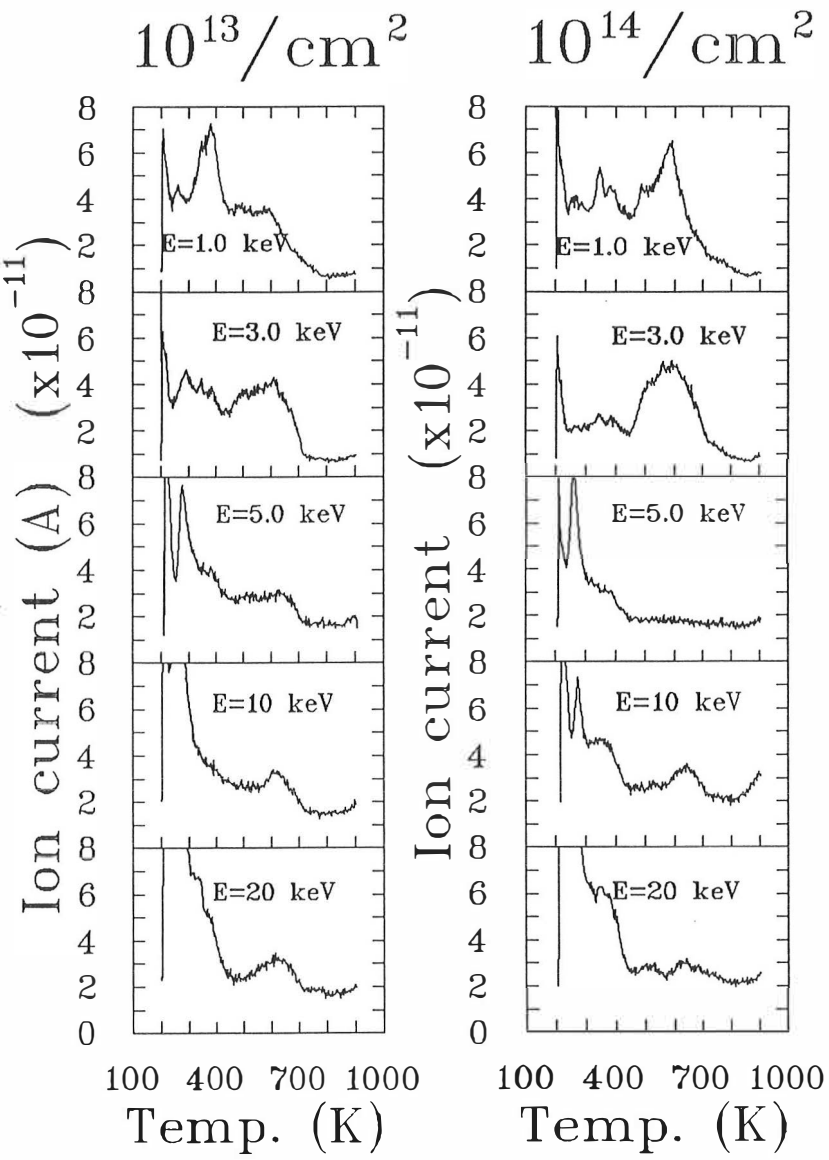

Figure 7.3. *Helium desorption from a copper single crystal, bombarded with* Ar *ions using the energies and doses indicated. The bombardment was followed by a helium injection with* 0.3 keV *helium* ($10^{13}/cm^2$). *The spectra were recorded with a heating rate of* 1.0 K/s.

The most striking feature is the absence of the H peak, in spite of the fact that there are certainly vacancies present because of the irradiation procedure. Secondly, the effects that may be regarded as consequences of the irradiation are observed only when using relatively low energies (1 - 3 keV) for Ar bombardment. This implies that the process is controlled by the limited range of injected helium atoms. When the bombarding energy is about 10 keV or higher, the only effect is the trace characteristic of 0.3 keV helium (see Fig. 5.1.)

The most visible effect due to argon irradiation is the one obtained for the bombarding energy of 3.0 keV. However, the distribution that can be interpreted as a fingerprint of the defects is a sum of many contributing processes, and the deconvolution of the spectrum to extract some of the defects discussed in chapter 5. is nearly impossible. Moreover, the maximum of the distribution in question is at 600 K, while the spectrum otherwise indicates a total absence of helium-filled monovacancies, i.e. the H peak does not exist in the spectrum.

When metals are irradiated with energetic particles, many kinds of defects are created. Generally, the lower is the ability for incoming ions to transfer energy to recoils, the higher is the probability to create monovacancies rather than larger defects [**93**]. It is well known that when irradiating metals with MeV-range electrons, pure monovacancies are formed, whereas irradiation with light ions creates a significant amount of double vacancies or larger defect complexes [**91**].

In this particular case, when a copper target is exposed to argon ions, the efficiency to transfer energy to recoils is relatively high. If a head-on collision is assumed, Eq. (5.1.) gives the result that 95 % of the kinetic energy of the incoming argon ion is transferred to the primary knock-on atom (PKA). This means that argon ions loose their energy within a few tens of atomic layers, and there is a considerable probability to create double vacancies or larger defects.

As mentioned in chapter 5.2., the peak temperature of the X peak, that was associated with helium release from singly-filled double vacancies, is 610 K. Therefore it is obvious that this peak participates in the helium-probing spectrum in the case of 3.0 keV argon. Due to the presence of argon, there are monovacancies and double vacancies filled with variable amounts of argon and helium. Evidently, the dissociation energies of these complexes differ from those discussed in chapter 5.3. Taking into consideration these facts,

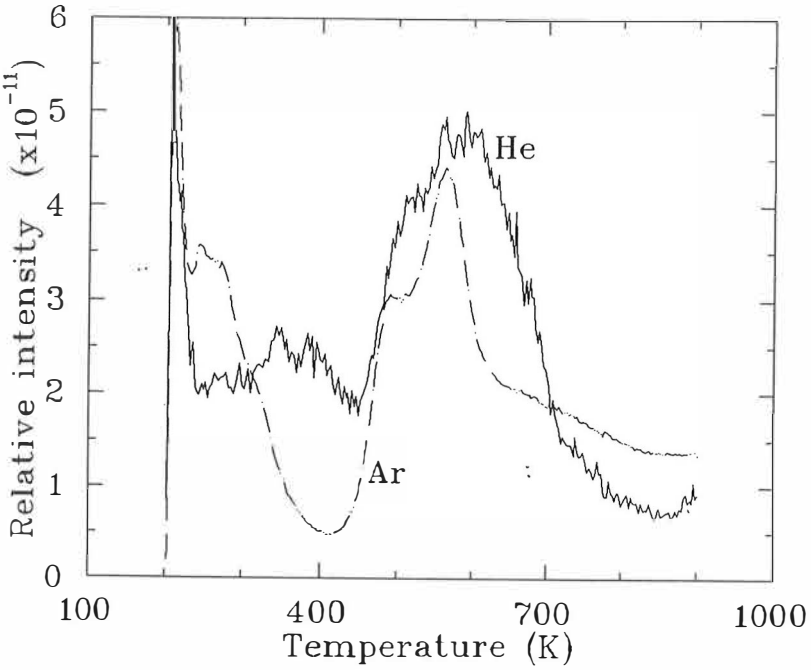

Figure 7.4. *Helium release (solid line) and argon release (dashed line) vs temperature after irradiating a copper target with* $10^{13}/cm^2$ 3.0 keV Ar^+ *ions followed by a helium injection with* $10^{13}/cm^2$ 0.3 keV He^+ *ions.*

the complexity of the helium-probing spectra can be understood.

In fact, the helium release monitored in helium-probing experiments coincides with the corresponding argon release as illustrated in Fig. 7.4. There is, however, a slight shift, i.e. the helium distribution reaches its maximum after the appearance of the double peak of argon. The irradiations were made at 200 K and the gas release was measured with a heating rate of 1.0 K/s. The effect has been observed previously when applying the same procedure on nickel [87].

The absence of the H peak means that the trapping of helium by pure monovacancies is strongly suppressed. This observation might be explained by the thermal spikes occuring during the heavy-ion bombardment. As mentioned in chapter 7.1., there is some evidence to assume that the influence of thermal spikes can be observed beyond the range of the argon implants. It is therefore possible that a major fraction of the vacancies annihilate because of row collisions. The anomaly concerning the missing H peak is discussed in

more detail in chapter 8.

When bombarding the sample with argon, the range of argon ions is only a few tens of atomic layers, and the corresponding vacancy profile is even closer to the surface. It was suspected that the distribution of injected helium overlaps the argon distribution while the region containing vacancies is not occupied by helium. To investigate this possibility, the irradiations were made using neon beams. Some THDS spectra obtained from such experiments are shown in Fig. 7.5.

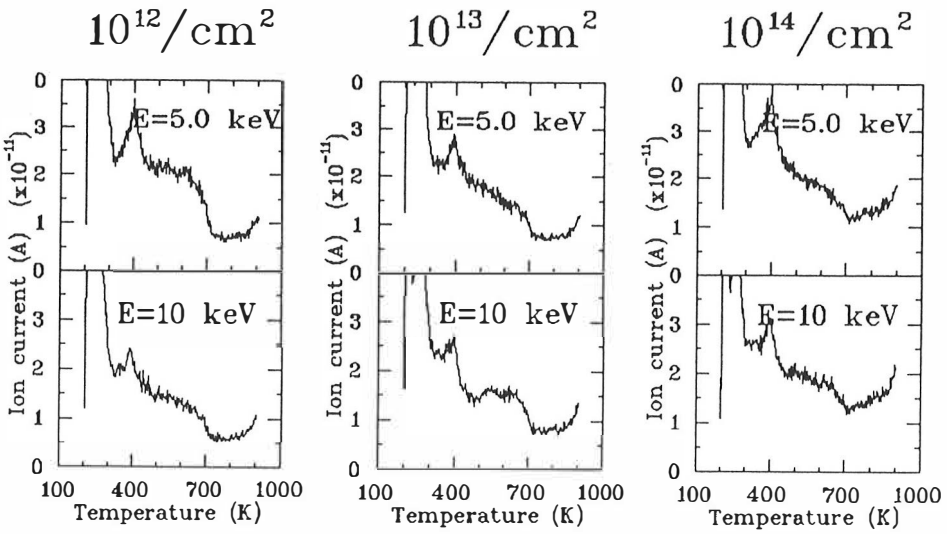

Figure 7.5. *THDS spectra from a copper single crystal irradiated with* Ne *ions and subsequently injected with* 0.3 keV *helium* ($10^{13}/cm^2$).

According to the TRIM calculation, the penetration of Ne is essentially higher in copper when compared to argon implanted with the same energy. In the case of keV-range ions, the difference is roughly a factor of two. Moreover, as a result of the implantation, the neon profile, as well as the vacancy profile, form a broad distribution without a sharp damage region just below the surface.

Nevertheless, no clear indication concerning helium-filled monovacancies was observed. In fact, in the case of neon bombardments the traces of injected helium do not reveal any effects that might be associated with helium-filled point defects. It is possible that the vacancies created by neon bombardment exist so deep that they are beyond the range of the injected helium.

8. Discussion

8.1. Recovery stages in copper

The mechanisms of irradiation effects in copper have been relatively well investigated using for example resistivity measurements [**13,61**], positron-lifetime measurements [**94-96**] and the perturbed angular correlation (PAC) method [**90-92**]. The recovery stages in copper are presented in Fig. 8.1.

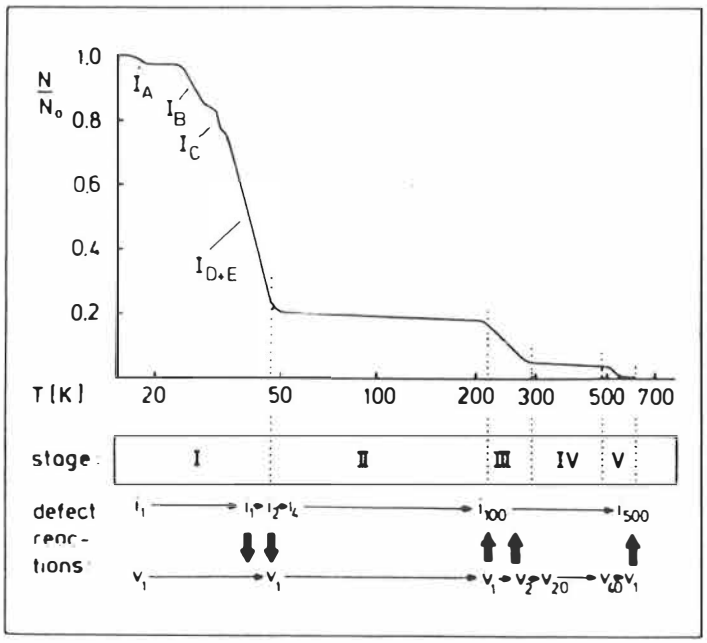

Figure 8.1. *Recovery stages of copper according to Schilling et al. [97].*

If the irradiation damage is created at a sufficiently low temperature, the first process, called the stage I, is observed at 40 K. This sequence is due to the mobilization of self-interstitials. In the particular case of copper, the activation energy for the migration of self-interstitials is 0.12 eV and the corresponding temperature is 38 K [**98**]. The next stage, called the stage II, can be associated with the growth of interstitial clusters leading

to small interstitial loops. In some metals the stage II can continue up to several hundreds of degrees kelvin [**61**].

There are two models for explaining the mechanism of the stage III in copper. The first one, called the vacancy model, assumes that vacancies become mobile at the stage III [**99-101**], whereas the other interpretation, called the two interstitial model, supposes that a fraction of self-interstitial atoms, called <100> dumb-bells, can survive at the stage II, and the processes at the stage III are due to annihilation of the dumb-bells at vacancies [**102,103**]. A majority of the scientists working in this field of condensed matter physics tend to prefer the vacancy model.

In the case of copper, the stage III is observed when the temperature is 220 - 330 K [**12,61,90**]. The activation energy for the stage III has been determined to be 0.72 eV [**70**]. The next stage (the stage IV) is due to growth of vacancy clusters. The corresponding temperature range covers from 330 K up to 450 K. Finally, at the stage V, the vacancy clusters dissociate and all damage is removed. The recovery process in copper is completed at 650 K [**94**].

Thermal helium desorption method can be mainly applied when investigating the temperature scale at the stage III or at higher temperatures. As mentioned previously in this text, it is difficult to combine the sample-cooling option with the other instrumentation problems concerning the THDS method. Therefore this method can usually not be applied to investigate the mobility of self interstitials, because these phenomena occur at 50 K or below, which is beyond the temperature region of typical THDS measurements.

The results obtained in this work indicate that the trapping of helium in copper monovacancies can be observed only when helium is implanted using keV-range energies, which makes it possible to push a lattice atom to interstitial position. By contrast, the widely used helium-probing technique (HPT) tends to give results that are difficult to interpret and there is no clear indication of helium-filled monovacancies, regardless of the fact that the experiments were carried out in such conditions in which pure vacancies can survive.

There is a lot of experimental evidence that the level of radiation damage in copper is strongly reduced during the stage I, that is, the recovery favours the interstitial mechanism [**89,90,104**]. Although the process depends on the projectiles used in the irradiation, up to 90 % of the initial damage has been found to disappear during the stage I annealing. This is a common trend for many FCC metals [**104**]. Based on this, it is possible that the

number of vacancies created at 200 K is essentially reduced by spontanous recombination with self-interstitials. It should be noted that a fraction of the irradiations were performed well below 200 K, but the results were exactly the same.

The row-collision mechanism caused by <100> dumb-bells might be a reasonable explanation for the problem of missing monovacancies. The existence of row collisions has been observed when investigating copper surfaces by means of molecular dynamics simulation [**105**].

The FCC structure of copper might be one reason why the helium atoms, injected with a subthreshold energy, are not trapped by pre-existing point defects. Compared with the BCC structure, the FCC structure has a higher three dimensional packing density, and the overlap of the surface atoms in any FCC metal is usually higher. Moreover, the packing density of copper atoms is very close to the theoretical packing density of the FCC structure, a feature common to all noble metals [**106**].

Because of the FCC structure, a copper vacancy is surrounded by 12 nearest neighbours, which means that the vacancy is strongly screened by them. There is also some experimental data to indicate that a copper vacancy is relaxed inwards [**107**], which increases the screening effect. Nevertheless, the shrinkage of a copper vacancy has not been observed when performing molecular dynamics simulations [**108**], and hence the experimental observations might have been wrongly interpreted.

The limited mobility of interstitial helium in copper is probably not the main reason for the failure in helium-probing experiments, although in the case of copper the migration energy of helium is very close to the activation energy of the stage III. As mentioned in chapter 5.5., the trapping propability of keV-range helium was found to increase when irradiated at low temperatures. This implies that vacancies are immobile and interstitial helium is mobile at 200 K, and the failure in helium-probing experiments is caused by some other reasons.

Finally, it is fully possible that the irradiation with heavy ions simply favours the formation of larger defect complexes rather than pure monovacancies. Since argon and neon impurities act also as a traps for helium, particularly because they are usually surrounded by vacancies, a helium desorption spectrum consists of many peaks having nearly the same activation energies. Therefore the spectra are very complicated and very difficult to deconvolute to separated peaks.

8.2. Helium-implanted copper

The interpretation of the defects created by keV-range helium implantation is nearly complete, with the exception that the nature of the X peak is more or less contradictional. It is clear that the X peak has something to do with divacancies, and the main question is whether the defect is filled with one or two helium atoms. Otherwise the interpretation is in accordance with the one discussed by Buters et al. [**68**]. The formation of relatively stable helium clusters was clearly observed when using high doses.

The activation energy (dissociation energy) for a He-vacancy complex was found to be $\geq$ 2.0 eV. The peak-area method as well as the Arrhenius fitting method gave a slightly higher values for the activation energy, and especially in the case of the Arrhenius method an unreasonable value for the rate constant was obtained. On the other hand, the limitations to attain accurate values for the kinetic parameters were clearly demonstrated.

In the case of ^{3}He measurements, the activation energy was nearly the same as the one obtained from ^{4}He experiments. The isotope effect was not clearly demonstrated because its influence, as predicted by the kinetic theory, is so tiny that it is hardly within the accuracy of the temperature measurement. When using the ^{3}He isotope, the temperature of the H peak was found to decrease, even though the rate constant, extracted from a peak-fitting procedure, was not exactly in accordance with the kinetic theory.

The dissociation energy for the H peak, according to the peak-fitting procedure, was found to be $E_D = (2.0 \pm 0.1)$ eV with the corresponding rate constant of $\nu_o = 10^{13.3 \pm 0.8}$ 1/s. The value of the rate constant is reasonable when compared to the Debye frequency of copper ($7 \cdot 10^{12}$ 1/s). The dissociation energy is in good agreement with theoretical predictions [**27,29,109**]. The experimental value determined by Buters et al. [**68**] was also 2.0 eV. The reason why the other analysing methods tend to give slightly higher values for the activation energy was not found. Evidently, the Arrhenius fitting procedure is modified by slight errors in temperature measurement.

The behaviour of helium implants in copper has been previously investigated mainly by using the perturbed angular correlation (PAC) method [**40,90-92,110-114**]. In these experiments a copper single crystal was implanted with 350 keV radioactive ^{111}In atoms followed by an annealing treatment at 800 K. Next the sample was implanted with 30

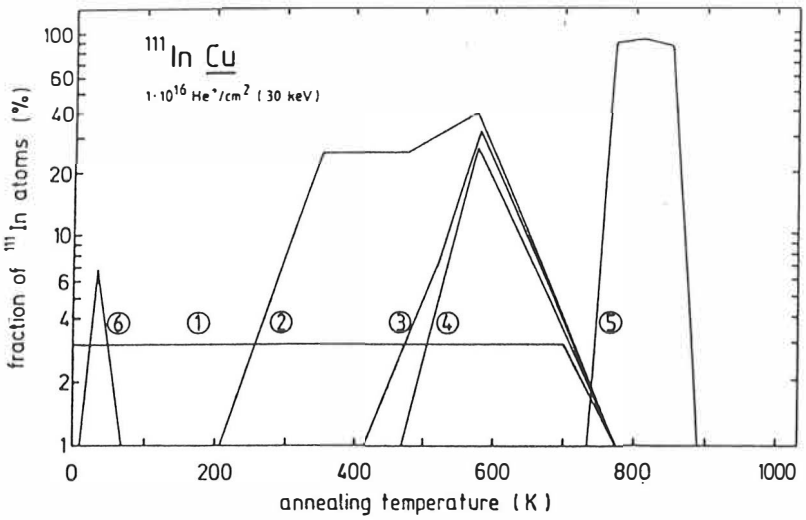

Figure 8.2. *Helium in copper studied by using the PAC technique [**114**].*

keV He^+ ions at 10 K, and various PAC spectra were measured at different annealing temperatures [**40,114**]. An interpretation of the results is shown in Fig. 8.2.

According to Wichert [**114**], the different components in the PAC spectra can be interpreted as follows. The first complex is formed at the irradiation temperature and it remains stable up to 700 K. This defect has to be a helium-filled monovacancy. The components 2-4 are interpreted as small helium clusters. The defect number 5 presumably corresponds to a helium bubble. Finally, the defect marked with number 6 is suspected to be due to interstitial migration of He in copper.

The interpretation of the components 1, 2 - 4 and 5 agree with the results obtained in this work. Evidently they represent the H, G and I peaks observed in the helium desorption spectra, respectively. The onset temperatures of the components observed in the PAC spectra are in agreement with the corresponding peak temperatures in helium desorption measurements.

The interpretation of the defect 6 can be put in question. If interstitial helium in copper were mobile at 25 K, the theoretical migration energy would be overestimated by a factor of 10, which is hard to believe. Moreover, the temperature in which helium becomes mobile in copper would be lower than in any other metal studied so far. Therefore it is possible that the interpretation of this defect is not correct.

It should be noted that the complex number 6 reaches its maximum at 30 K [**40**] which is very close to the stage I in copper. This implies that the formation of this complex is caused by a kick-out reaction, when a substitutional helium atom is replaced by a mobile self-interstitial and the helium atom is pushed to interstitial position (see Eq. (7.1.)). The interstitial helium atom is finally observed as a perturbation in the electric field gradient of a radioactive ^{111}In probe atom. According to theoretical calculations [**29**], the process is energetically possible, that is, the total energy of a system containing a substitutional helium atom and one copper self-interstitial is higher than the formation energy of interstitial helium in copper.

8.3. Interstitial diffusion of helium in copper

The PAC experiments described above indicate also that a certain defect complex containing helium is formed after 200 K (component 2 in Fig. 8.2.). If this complex were due to interstitial migration of helium in copper, it would be in agreement with the theoretical calculations. Actually, this observation was the main motivation for the attempts to determine the migration energy of helium in copper by means of desorption experiments.

The results obtained from low-temperature measurements indicated that interstitial helium is mobile at 200 K. Therefore it is possible that the observed helium release at 180 K is not a reliable indicator for the determination of the migration energy of helium. Evidently the investigations of helium diffusion are beyond a reasonable operating temperature range of the desorption facility.

Van der Kolk et al. [**69**] have bombarded a copper <110> single crystal with 3.0 keV He^+ ions at low temperatures and measured the corresponding desorption spectrum. At the very beginning of the heating procedure, a broad helium-release distribution was obtained between 200 K and 400 K when using a heating rate of 40 K/s. If this peak is due to interstitial migration of helium in copper, the corresponding migration energy is 0.50±0.05 eV, derived from our diffusion model. Hence the value is more than 0.1 eV higher than the one obtained in our measurements. The authors gave no explanation for this observation, and it might also be a surface effect, since the sample surface is very sensitive to impurity adsorbants at low temperatures.

When the thermal desorption method is applied to diffusion experiments, the only reasonable observable to be extracted is the onset temperature at which the impurities become

mobile. The determination of the corresponding migration energy is evidently sensitive to the model used in the interpretation. The model described in chapter 2.3. is probably too simple to explain the physical phenomena behind the diffusion process.

The diffusion process may depend on the orientation of the target crystal. For example, in the case of FCC metals, the <110> channel is, according to simple geometrical arguments, the most effective way to attain the maximum implantation depth, whereas the <111> surface has an essentially higher packing density. Moreover, if there are more than one impurity in the same interstitial position, the stability of such a complex is different from the one of a singly-filled interstitial site .

Finally, the presence or absence of vacancies may affect the diffusion process. Since helium is practically insoluble in metals, the only way to introduce helium in a perfect metal lattice is the implantation below the displacement threshold energy. Another widely used method is the tritium trick [**115**], which is based on the formation of ^{3}He via the disintegration of tritium

$$^3H \rightarrow {}^3He + e^- + \bar{\nu}. \qquad (8.1.)$$

The role of intrinsic vacancies in the diffusion process depends on the character of the metal and on the impurity in question. It is well known that in some metals the diffusion of oversized impurities may be assisted by vacancies. In the case of helium in metals, vacancies are of hindrance rather than of assistance, because helium-filled vacancies are more stable than vacancies or interstitial helium atoms alone.

8.4. Ne and Ar implants in copper

The desorption of argon and neon from copper turned out to be a relatively complicated process that can not be described by simple first-order rate equations. Furthermore, the identification of each peak is essentially more difficult than in the case of helium-filled defects. The most striking feature was the double peak appearing in the case of both argon and neon, especially because the results indicated that neon might be more deeply bound in the defects than argon.

As indicated in Ref. [**83**], the desorption peaks of argon and neon have something to do with vacancies, because the intensity of the peaks can be essentially reduced by introducing self-interstitials by heavy-ion bombardment. The main question is what is the actual role of vacancies in the case of neon and argon implants.

Reintsema et al. have investigated the recovery of Xe in molybdenum by means of Mössbauer spectroscopy [**116**]. They concluded that heavy noble gas implants are always trapped by clusters containing a variable amount of vacancies. The stability of a cluster depends mainly on the three-dimensional symmetry of the cluster and it does not show a simple trend as a function of the number of vacancies only. Therefore, XeV and XeV_4 were found to be the most stable defect complexes, whereas XeV_2 and XeV_3 are essentially weaker.

The interpretation presented by Reintsema et al. has been criticized by van der Kolk et al. [**117**] because the effects, observed in the Mössbauer spectra, can be explained by the vacancies appearing in the first- or second-neighbour positions. This explanation is based on the fact that there are always a large number of vacancies in the vicinity of implanted heavy noble gas impurities.

Evidently, the desorption peaks in neon and argon spectra are spread for two reasons. Firstly, the defects are usually vacancy complexes rather than monovacancies and they tend to move by diffusion mechanism. A fraction of the defects annihilate at the surface. Secondly, during the diffusion process a defect can capture or loose a vacancy, which means that the number of certain defects is fluctuating with time. Taking into consideration these aspects, it is natural that the desorption of neon and argon can not be described by means of the single-jump rate equation as in the case of helium filled vacancies.

8.5. On the validity of the THDS method

Thermal helium desorption method is a valuable tool to extract information on the microscopic processes of radiation damage. However, it is not a very suitable method to be applied to low-melting materials. Due to limited penetration of the helium ions, the method is insensitive to phenomena that occur deeper than, say, 100 atomic layers beneath the surface. On the other hand, the sample has to tolerate relatively high temperatures and repeated heating-cooling cycles.

The most reasonable way to obtain a complete picture on the microscopical irradiation effects is to compare the results of the THDS method with the data obtained from other experimental or theoretical investigations. In this work the results of helium desorption experiments are in good agreement with the PAC measurements. The perturbed angular correlation method, as well as positron-lifetime measurements and resistivity measurements can give complementary information of low-temperature effects, because the THDS method is difficult to apply when performing measurements far below room temperature. If the main interest is concentrated on the phenomena that occur very close to the surface, it might be convenient to couple a THDS facility with slow positron beams.

9. Summary

This thesis is a pilot project to apply the THDS method in Jyväskylä. The project included the construction of the helium desorption facility, first-principle measurements on copper and the analysis of the results.

Some attention was paid to the details of the data analysis based on first-order kinetics. It turned out that there are many alternative methods for analysing the data, and the classical method based on the peak shift with different heating rates is not the only one, and in some cases it is not the most reliable one either. The peak-area method, as well as the peak-width method, described in chapter 3, are applicable when using relatively low heating rates.

The desorption facility has turned out to be a reliable and low-cost instrument. The lack of a surface-analysis instrument (LEED, for example) is the worst bottleneck when performing further investigations. Some improvements have to be made concerning the gas ion source; a differentially pumped version with a mass analysis would be an essentially better solution. The calibration system has to be completed if it is really expected to be necessary. It should be noted that a great amount of useful information can be obtained just by analysing the relative intensities of desorption spectra. The sensitivity of the mass spectrometer does not vary critically as a function of time, and the reproducibility of the experiments is rather good.

The behaviour of helium in copper can be rather well understood. Helium release from copper vacancies can be clearly observed, and it was found to obey first-order kinetics. All the peaks appearing in helium desorption spectra can be identified. The release of other noble gases tends to be a more complicated process which can not be described by simple rate equations. Evidently, these phenomena are associated with noble-gas-filled defect agglomerates consisting of a variable amount of vacancies.

When the THDS method was applied to probe defects created by argon or neon beams, no helium-filled monovacancies were observed. It is possible that the irradiation procedure creates mainly larger defects than pure monovacancies, or there is some peculiar mechanism to suppress the creation of point defects in copper. It is possible that majority of the defects is recovered by interstitial mechanisms.

References

[1] E.V. Kornelsen, Can. J. Phys **42**, 364 (1964).

[2] K. Erents, R.P.W. Layson and G. Carter, J. Vac. Sci. and Tech. **4**, 252 (1966).

[3] E.V. Kornelsen and M.K. Sinha, J. Appl. Phys. **39**, 4546 (1968).

[4] E.V. Kornelsen and M.K. Sinha, J. Appl. Phys. **40**, 2888 (1969).

[5] E.V. Kornelsen, Can. J. Phys. **48**, 2812 (1970).

[6] J.F. O'Hanlon, *A Users Guide to Vacuum Technology* (John Wiley & Sons, New York, 1980) p. 247.

[7] G.J. van der Kolk, (Ph. D. Thesis, Delft University of Technology, Delft, 1984).

[8] W.T. Moore and E.V. Kornelsen, Radiat. Eff. **90**, 141 (1985).

[9] S.K. Erents and G. Carter, Brit. J. Appl. Phys. (J. Phys. D) **1**, 1323 (1968).

[10] E.V. Kornelsen, Radiat. Eff. **13**, 227 (1972).

[11] A.A. van Gorkum and E.V. Kornelsen, Vacuum **31**, 89 (1981).

[12] A. van Veen, Materials Science Forum **15-18**, 3 (1987).

[13] L.M. Stals, in *Site Characterization and Aggregation of Implanted Atoms in Materials*, edited by A. Perez and R. Coussement (Plenum Press, New York, 1980) p. 357.

[14] H. Rajainmäki, S. Linderoth, H.E. Hansen, R.M. Nieminen and M.D. Bentzon, Phys. Rev. B **38**, 1087 (1988).

[15] S. Mäkinen, H. Rajainmäki and S. Linderoth, Phys. Rev. B **42**, 11166 (1990).

[16] P. Hautojärvi (ed.), *Positrons in Solids*, Volume 12 of *Topics in Current Physics* (Springer, Heidelberg, 1979).

[**17**] H.E. Hansen, R. Talja, H. Rajainmäki, H.K. Nielsen, B. Nielsen and R.M. Nieminen, Appl. Phys. A **36**, 81 (1985).

[**18**] P.A. Redhead, Vacuum **12**, 203 (1962).

[**19**] G. Garter, Vacuum **12**, 245 (1962).

[**20**] M. Abramovitz and I.A. Stegun, *Handbook of Mathematical Functions* (Dover, New York, 1970).

[**21**] J. Timonen, private communication.

[**22**] P.W. Atkins, *Physical Chemistry*, Third Edition (Oxford, 1986) p. 694.

[**23**] W. Schilling, in *Point Defects and Defect Interaction in Metals*, edited by J-I. Takamura, M. Doyama and M. Kiritani (University of Tokyo Press, 1982) p. 303.

[**24**] W.D. Wilson and R.A. Johnson, in *Interatomic potentials and simulation of lattice defects*, edited by P.C. Gehlen, J.R. Beeler and R.I. Jaffee (Plenum Press, New York, 1972) p. 375.

[**25**] D.J. Reed, Radiat. Eff. **31**, 129 (1977).

[**26**] W.D. Wilson and C.L. Bisson, Phys. Rev. B **3**, 3984 (1971).

[**27**] W.D. Wilson, M.I. Baskes and C.L. Bisson, Phys. Rev. B **13**, 2470 (1976).

[**28**] C.F. Melius, C.L. Bisson and W.D. Wilson, Phys. Rev. B **18**, 1647 (1978).

[**29**] M.I. Baskes and C.F. Melius, Phys. Rev. B **20**, 3197 (1979).

[**30**] W. D. Wilson, C.L. Bisson and M.I. Baskes, Phys. Rev. B **24**, 5616 (1981).

[**31**] B. Bech Nielsen and A. van Veen, J. Phys. F: Met. Phys. **15**, 2409 (1985).

[**32**] S.T. Picraux, Nucl. Instr. Meth. **182/183**, 413 (1981).

[**33**] B.M.U. Scherzer, in *Sputtering by Particle Bombardment II*, edited by R. Behrisch (Springer, Heidelberg, 1983) p. 271.

[**34**] A. Wagner, D.N. Seidman, Phys. Rev. Letters **42**, 515 (1979).

[**35**] G.J. Thomas, W.A. Swasinger and M.I. Baskes, J. Appl. Phys. **50**, 6942 (1979).

[**36**] V. Philips, K. Sonnenberg and J.M. Williams, J. Nucl. Mat. **107**, 271 (1982).

[**37**] D.B. Poker and J.M. Williams, Appl. Phys. Lett. **40**, 851 (1982).

[**38**] G.J. Thomas and R. Bastasz, J. Appl. Phys. **52**, 6426 (1981).

[**39**] M. Deicher, G. Grübel, E. Recknagel, W. Reiner and Th. Wichert, Mater. Sci. & Eng. **69**, 57 (1985).

[**40**] Th. Wichert, M. Deicher, G. Grübel, E. Recknagel and W. Reiner, Phys. Rev. Lett. **55**, 726 (1985).

[**41**] G.J. Thomas, Radiat. Eff. **78**, 37 (1983).

[**42**] L.A. Girifalco, *Atomic Migration in Crystals* (Blaisdell Publishing Company, New York, 1964) p. 56.

[**43**] R.J. Borg and G.J. Dienes, *An Introduction to Solid State Diffusion* (Academic Press, San Diego, 1988) p. 5.

[**44**] M. Alonso, E.J. Finn, *Fundamental University Physics, Volume II Fields and Wawes*, 9th Edition (Addison-Wesley, Reading, Mass. 1978) p. 934.

[**45**] M. Alonso, E.J. Finn, *Fundamental University Physics, Volume III Quantum and Statistical Physics* (Addison-Wesley, Reading, Mass. 1982) p. 517.

[**46**] J.L. Falconer and R.J. Madix, Surf. Sci. **48**, 393 (1975).

[**47**] J. Kuhalainen, Ph. Lic. thesis (Laboratory Report 2/1994, Department of Physics, University of Jyväskylä, 1994, in Finnish).

[**48**] D.H. Parker, M.E. Jones and B.E. Koehl, Surf. Sci. **233**, 65 (1990).

[**49**] A.M. de Jong and J.W. Niemantsverdried, Surf. Sci. **233**, 355 (1990).

[**50**] A.A. van Gorkum, J. Appl. Phys. **51**, 2594 (1981).

[**51**] R. Chen, J. Appl. Phys. **40**, 570 (1969).

[**52**] D. Edwards, Jr., Surf. Sci. **54** 1 (1976).

[**53**] C-M. Chan, R. Aris and W.H. Weinberg, Appl. Surf. Sci. **1**, 360 (1978).

[**54**] J.L. Falconer and J.A. Schwarz, Catal. Rev. Sci. Eng. **25**, 141 (1983).

[**55**] E.V. Kornelsen and A.A. van Gorkum, Vacuum **31**, 99 (1981).

[**56**] E.V. Kornelsen and D.L. Blair, J. Vac. Sci. Technol. **14,** 1299 (1977).

[**57**] A. van Veen, A. Warnaar and L.M. Caspers, Vacuum **30**, 109 (1980).

[**58**] E. Kautto, O-P. Kähkönen, J. Kuhalainen and M. Manninen, accepted for publication in Nucl. Instr. Meth. B.

[**59**] H. Enosawa, C. Urano, T. Kawashima and M. Yamamoto, J. Vac. Sci. Technol. A **8**, 2768 (1990).

[**60**] O-P. Kähkönen, E. Kautto and M. Manninen, J. Appl. Phys. **72**, 2075 (1992).

[**61**] P. Ehrhart, K.H. Robrock and H.R. Schober, in *Physics of Radiation Effects in Crystals*, Volume 13 of *Modern Problems of Condensed Matter Sciences*, edited by R.A. Johnson and A.N. Orlow (North Holland, Amsterdam, 1986) p. 3.

[**62**] J. Ärje, H. Koivisto and M. Nurmia, in *Proceedings of the 11th International Workshop on ECR Ion Sources*, KVI Report **996** (1993).

[**63**] H. Koivisto, J. Ärje and M. Nurmia, Nucl. Instr. Meth. B **94**, 1291 (1994).

[**64**] S.G.J. Mochrie, Phys. Rev. Lett. **59**, 304 (1987).

[**65**] D. Gorse and J. Lapujoulade, Surf. Sci. **162**, 847 (1985).

[**66**] S. Thevuthasan and W.N. Unertl, Appl. Phys. A **51**, 216 (1990).

[**67**] J. Merikoski, H. Häkkinen, M. Manninen and J. Timonen, Phys. Rev. B **49**, 4938 (1994).

[**68**] W.Th.M. Buters, A. van Veen and A. van den Beukel, Phys. Stat. Sol. (a) **100**, 87 (1987).

[**69**] G.J. van der Kolk and A. van Veen, Physica Scripta **T13**, 53 (1986).

[70] J. Leteurtre, in *Site Characterization and Aggregation of Implanted Atoms in Materials*, edited by A. Perez and R. Coussement (Plenum Press, New York, 1980) p. 265.

[71] G.H. Kinchin R.S. Pease, Rep. Prog. **18**, 1 (1955).

[72] A. van Veen, J.H. Evans, L.M. Caspers and J.Th.M. de Hosson, J. Nuclear Mater. (Amsterdam) **122/123**, 560 (1984).

[73] E.V. Kornelsen and D. Edwards, Jr., in *Applications of Ion Beams to Metals*, edited by S.T. Picraux, E.P. Eernisse and F.L. Vook (Plenum Press, New York, 1974) p. 521.

[74] J.F. Ziegler, J.P. Biersack and U. Littmark, *The Stopping and Range of Ions in Solids* (Pergamon Press, New York, 1985).

[75] D. Edwards, Jr., J. Appl. Phys. **46**, 1437 (1975).

[76] D. Edwards, Jr., J. Appl. Phys. **46**, 1444 (1975).

[77] E.V. Kornelsen and M.K. Sinha, Can. J. Phys. **46**, 613 (1968).

[78] H. Häkkinen, private communication.

[79] B. Perovic and T. Jokic, Phys. Letters **20**, 485 (1966).

[80] T. Jokic and B. Perovic, Can. J. Phys. **46**, 635 (1968).

[81] J.Th.M. de Hosson, Phys. Stat. Sol. A **40**, 293 (1977).

[82] A. van Veen, W.Th.M. Buters, G.J. van der Kolk and L.M. Caspers, Nucl. Instr. Meth. **194**, 485 (1982).

[83] A. van Veen, W.Th.M. Buters, T.R. Amstrong, B. Nielsen, K.T. Westerduin, L.M. Caspers and J.Th.M. de Hosson, Nucl. Instr. Meth. **209/210**, 1055 (1983).

[84] K. Jacobsen, J. Nørskov and M. Puska, Phys. Rev. B **35**, 7423 (1987).

[85] G.J. van der Kolk, A.S. Hydra, A. van Veen and L. M. Caspers, Nucl. Instr. Meth. **209/210**, 1047 (1983).

[86] G.J. van der Kolk, A. van Veen, J.Th.M. de Hosson and L.M. Caspers, Nucl. Instr. Meth. B **6**, 517 (1985).

[87] B. Bailey, D.G. Armour, D.S. Karpuzov and G. Carter, Radiat. Eff. **78**, 133 (1983).

[88] J.R. Fransens, F. Pleiter and J.M. Meinders, Hyp. Int. **60**, 745 (1990).

[89] H. Metzner, R. Sielemann, S. Klaumünzer and E. Hunger, Materials Science Forum **15 - 18**, 1063 (1987).

[90] M. Deicher, G. Grübel, R. Minde, E. Recknagel and Th. Wichert, in *Point Defects and Defect Interaction in Metals*, edited by J-I. Takamura, M. Doyama and M. Kiritani (University of Tokyo Press, 1982) p. 220.

[91] M. Deicher, G. Grübel, E. Recknagel, W. Reiner and Th. Wichert, in *Microstructural Characterization of Materials by Non-Microscopical Techniques*, edited by N. Hessel Andersen, M. Eldrup, N. Hansen, D. Juul Jensen, T. Leffers, H. Lilholt, O.B. Pedersen and B.N. Singh (Risø National Laboratory, Roskilde, 1984) p. 225.

[92] Th. Wichert, Materials Science Forum **15 - 18**, 829 (1987).

[93] R. Bullough and M.H. Wood, in *Physics of Radiation Effects in Crystals*, Volume 13 of *Modern Problems of Condensed Matter Sciences*, edited by R.A. Johnson and A.N. Orlow (North Holland, Amsterdam, 1986) p. 189.

[94] S. Mantl and W. Triftshäuser, Phys. Rev. Lett. **34**, 1554 (1975).

[95] R.H. Howell, Phys. Rev. B **18**, 3015 (1978).

[96] M.J. Fluss, L.C. Smedskjaer, R.W. Siegel, D.G. Legini and M.K. Chason, J. Phys. F: Met. Phys. **10**, 763 (1980).

[97] W. Schilling, P. Ehrhart and K. Sonnenberg, in *Fundamental Aspects of Radiation Damage in Metals*, Vol. P1, edited by M.T. Robinson and F.W. Young (US Energy Research and Development Administration, Conf.-751006, 1975) p. 470.

[98] F.W. Young, Jr., J. Nucl. Mater. **69/70**, 310 (1978).

[99] W. Schilling, G. Burger, K. Isebeck and H. Wenzl, in *Vacancies and Interstitials in Metals*, edited by A. Seeger, D. Scumacher, W. Schilling and J. Diehl (North-Holland, Amsterdam, 1970) p. 255.

[**100**] W. Shilling and K. Sonnenberg, J. Phys. F: Met. Phys. **3**, 322 (1973).

[**101**] J.W. Corbett, R.B. Smith and R.M. Walker, Phys Rev. **114**, 1452 (1959).

[**102**] A. Seeger, in *Vacancies and Interstitials in Metals*, edited by A. Seeger, D. Scumacher, W. Schilling and J. Diehl (North-Holland, Amsterdam, 1970) p. 999.

[**103**] W. Frank and A. Seeger, Radiat. Eff. **1**, 117 (1969).

[**104**] D. Segers, I. Lemahieu, L. Dorikens-Vanpraet, M. Dorikens and J. Paridaens, Phys. Lett. A **133**, 455 (1988).

[**105**] J. Merikoski, private communication.

[**106**] N.W. Ashcroft and N.D. Mermin, *Solid State Physics* (HRW International Editions, Philadelphia, 1981) p. 374.

[**107**] P. Erhart and U. Schlagheck, J. Phys. F: Met. Phys. **4**, 1589 (1974).

[**108**] H. Häkkinen, private communication.

[**109**] M. Manninen, J.K. Nørskov and C. Umrigar, J. Phys. F: Met. Phys. **12**, L7 (1982).

[**110**] M. Deicher, G. Grübel and Th. Wichert, Nucl. Instr. Meth. **209/210**, 817 (1983).

[**111**] F. Pleiter, A.R. Arends and H. de Waard, Phys. Lett. **77A**, 81 (1980).

[**112**] M. Deicher, G. Grübel, W. Reiner and Th. Wichert, Hyp. Int. **15/16**, 476 (1983).

[**113**] G. Grübel, M. Deicher, R. Keller, Th. Korinth, W. Reiner, E. Recknagel and Th. Wichert, Hyp. Int. **35**, 609 (1987).

[**114**] Th. Wichert, in *Characterization of Defects in Materials*, edited by R.W. Siegel, J.R. Weertman and R. Sinclair (Material Research Society, Pittsburgh, Pennsylvania, 1987) p. 35.

[**115**] J.R. Cost and R.G. Hickman, J. Vac. Sci. Technol. **12**, 516 (1975).

[**116**] S.R. Reintsema, E. Verbiest, J. Odeurs and H. Pattyn, J. Phys. F **9**, 1511 (1979).

[**117**] G.J. van der Kolk, A. van Veen and L.M. Caspers, Nucl. Instr. Meth. B **2**, 710 (1984).